

# Rapid Membrane-Penetrating Hybrid Peptides Achieve Efficient Dual Antimicrobial and Antibiofilm Activity through a Triple Bactericidal Mechanism

Yifan Liu,<sup>†</sup> Pengfei Cui,<sup>\*,†</sup> Rong Tan, and Shaoguo Ru<sup>\*</sup>Cite This: *ACS Omega* 2024, 9, 26133–26148

Read Online

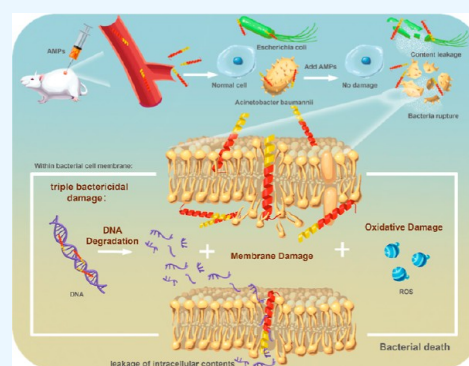
ACCESS |

Metrics &amp; More

Article Recommendations

Supporting Information

**ABSTRACT:** Antimicrobial peptides (AMPs) are a type of biomaterial used against multidrug resistant (MDR) bacteria. This study reports the design of a peptide family rich in tryptophan and lysine obtained by optimizing a natural AMP using single factor modification and pheromone hybridization to expedite the penetration and improve the antimicrobial activity of AMPs. S-4, L-4, and P-4 showed  $\alpha$ -helical structures, exhibited extremely fast membrane penetration rates *in vitro*, and could kill MDR bacteria efficiently within 30 min. Intracellular fluorescence localization suggested rapid membrane-penetrating of AMPs within 1 min, making it more difficult for bacteria to develop resistance. Furthermore, they could effectively inhibit and destroy bacterial biofilms with dual antimicrobial and antibiofilm activity. In the treatment of skin infections caused by MDR-*Acinetobacter baumannii* *in vivo*, AMPs could effectively alleviate inflammation without toxic side effects. Additionally, the triple antimicrobial damage of AMPs was described in detail. AMPs rapidly penetrate the cell membrane, inducing cell membrane damage, triggering oxidative damage with a storm of reactive oxygen species and leading to bacterial death through leakage of cellular contents by complexing with DNA. The multiple damage is an important means by which AMPs can prevent bacterial resistance adequately.



## 1. INTRODUCTION

Infections caused by “super bacteria” such as *Acinetobacter baumannii* that result from an overuse of antibiotics have become a major public health concern.<sup>1–4</sup> Antimicrobial peptides (AMPs) have emerged as an alternative to antibiotics because of their activity against multidrug-resistant (MDR) bacteria.<sup>5–8</sup> The structural differences between AMPs and antibiotics, such as secondary structures of  $\alpha$ -helix and  $\beta$ -fold,<sup>9</sup> and electropositive and amphiphilic properties,<sup>10,11</sup> lead to their unique membrane damage abilities and antibacterial mechanisms that could kill antibiotic-resistant bacteria. For *A. baumannii*, due to its high antibiotic resistance and biofilm formation capacity, several natural AMPs and synthetic AMPs have been developed to replace conventional antibiotics,<sup>12</sup> such as ZY4,<sup>13</sup> Octominin,<sup>14</sup> and Cec4.<sup>15</sup> However, the efficacy and toxic effects of newly developed antibiotic alternatives still need to be fully evaluated at the *in vivo* and *in vitro* levels to be suitable for clinical use.

Previous studies have shown that some AMPs, effective in killing planktonic bacteria, sometimes show unsatisfactory resistance to biofilms.<sup>16,17</sup> Some AMPs can inhibit biofilm formation to some extent and induce lysis of existing biofilms<sup>18,19</sup> but cannot efficiently kill planktonic bacteria. It takes more than 1.5–24 h for most AMPs to kill bacteria and biofilms completely.<sup>10,16,17</sup> The prolonged bactericidal time and incomplete mortality are important contributors to the

development of bacterial drug resistance. Currently, AMPs with dual antibacterial and antibiofilm activity that can efficiently and rapidly destroy MDR bacteria and biofilms are lacking. Therefore, it could compensate for the deficiency of AMPs and provide a reliable scheme for developing more efficient AMPs if the penetration rates could be increased to obtain antibacterial and antibiofilm activity that can quickly kill MDR bacteria.

However, a single membrane damage mechanism is insufficient to enhance the antibacterial and antibiofilm activity of AMPs against MDR bacteria;<sup>20,21</sup> nonspecific membrane affinity can lead to some hemolytic activity.<sup>22,23</sup> Although the typical action mechanism of AMPs involves the cell membrane, evidence suggests that some AMPs also have other intracellular targets that induce cell damage.<sup>24</sup> For example, MBP-1<sup>25</sup> isolated from wheat exhibited antibacterial activity attributed to its DNA-binding ability, whereas AMP KW4<sup>26</sup> demonstrated antifungal activity by binding to fungal DNA. Multiple antibacterial mechanisms can reduce the chances of developing

Received: February 19, 2024

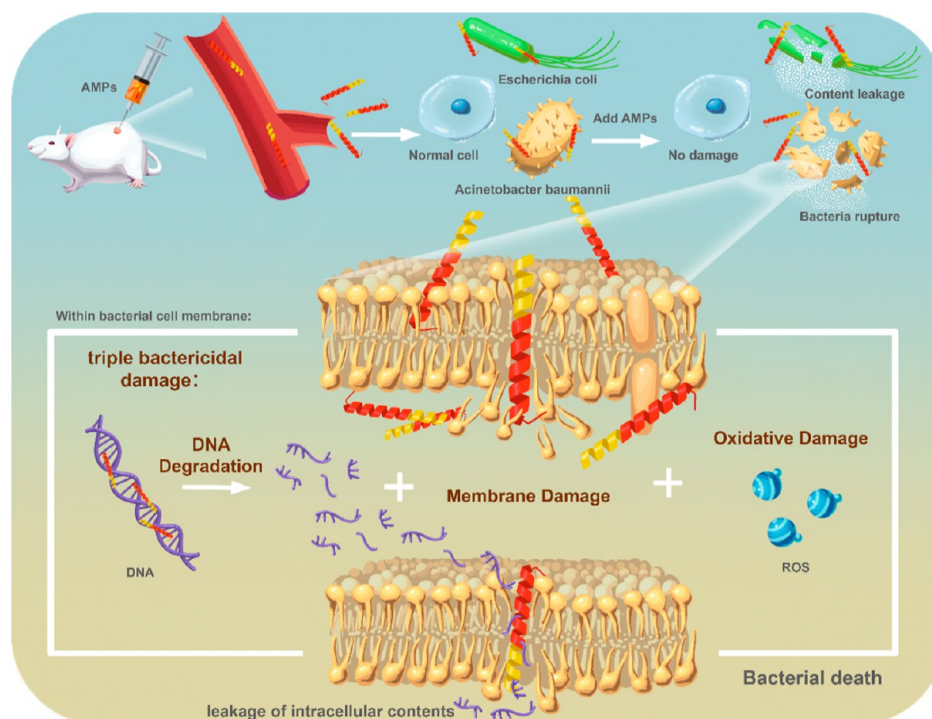
Revised: May 21, 2024

Accepted: May 24, 2024

Published: June 5, 2024



Scheme 1. Schematic Illustration of AMPs-Mediated Antibacterial Therapy



drug resistance and generate AMPs that rapidly kill MDR bacteria and biofilms. In addition to being associated with multiple mechanisms, the antibacterial and antibiofilm activities of AMPs depend on their bactericidal rate.<sup>27,28</sup> The bactericidal rate primarily depends on the penetration rate of AMPs. Therefore, we aimed to determine the penetration rate in bacteria and the possibility of binding to the intracellular DNA of AMPs using fluorescence tracing technology to elucidate its possible antibacterial mechanisms.

The performance of AMPs is primarily related to the net charge, hydrophobicity, and amphiphilicity and is the result of the coordination between various structural parameters.<sup>7</sup> Hybrid peptides can combine the advantages of different peptide chains to improve the structural parameters and secondary structure of AMPs, which is a simple and effective strategy for designing and optimizing AMPs.<sup>29</sup> The high membrane affinity and aggregation ability of bacterial pheromones enable them to stabilize the  $\alpha$ -helix structure and enhance the penetration speed;<sup>30</sup> therefore we proposed hybridizing bacterial pheromones with optimized AMPs to obtain  $\alpha$ -helical peptides with faster penetration. mBjAMP1<sup>31</sup> (NLCASLRARHTIPQCKKFGRR), a natural AMP discovered in our previous study, was modified and optimized to improve the antibacterial and antibiofilm activity and prevent the development of drug resistance through multiple antibacterial mechanisms. Lysine (K) carries a positive charge and can facilitate the tight binding of peptides to the negatively charged phospholipid layer of the cell membrane.<sup>32–34</sup> Hydrophobic tryptophan (W) enhances the affinity of the peptide for the cell membrane,<sup>35–37</sup> stabilizing the helical structure. Therefore, we synthesized AMP 1–4 (WKKWSKRWRHWIPQCKKFGRR) by introducing tryptophan (W) and lysine (K) as amino acid substitutions. This was an attempt to increase the binding force between AMPs and negatively charged cell membranes and DNA by improving the hydrophobicity and positive charge, with the hope of exerting multiple effects on bacterial cell

membranes and DNA, further prolonging the development of bacterial drug resistance. Following this, *Staphylococcus aureus*,<sup>38</sup> *Lactobacillus monoproliferis*,<sup>39</sup> and *Pseudomonas* pheromone fragments<sup>40</sup> were added at the N-terminus of 1–4 to construct S-4 (YSTCDFIMWKKWSKRWRHWIPQCKKFGRR), L-4 (ASSLLLVGWKKWSKRWRHWIPQCKKFGRR), and P-4 (KKHRKHRKRWKKWSKRWRHWIPQCKKFGRR). In addition to lengthening the  $\alpha$ -helix structure, the stability was enhanced to improve the rapid destruction ability of AMPs against bacteria and their biofilms. In this study, the antibacterial damage of the derived AMPs was explored, and the transmembrane speed of the AMPs was characterized. Similarly, the rapid membrane penetration characteristics of AMPs were systematically described, and the AMPs were applied to inflammatory diseases related to MDR bacterial infections (Scheme 1).

## 2. MATERIALS AND METHODS

**2.1. Materials.** Phosphate-buffered saline (PBS, powder) was purchased from BioSharp Life Sciences Co., Ltd. (Anhui, China); yeast extract and tryptone were purchased from Thermo Fisher Scientific Co., Ltd. (USA); nutrient broth (NB) and brain heart infusion (BHI) broth were purchased from Qingdao Hope Biotechnology Co., Ltd. (Qingdao, China); 2,2,2-Trifluoroethanol (TFE) was purchased from Sigma-Aldrich. (USA); dimethyl sulfoxide (DMSO) and 2',7'-dichlorodihydrofluorescein diacetate (DCFH-DA) were purchased from J&K Chemical Technology (Beijing, China); HEPES buffer was purchased from Shanghai Yuanye Biotechnology Co., Ltd. (Shanghai, China); 3,3'-dipropylthiadicarbocyanine Iodide (DiSC<sub>3-5</sub>) was purchased from AAT BioQuest Co. Ltd. (USA); methanol, absolute ethanol, 25% aqueous glutaraldehyde solution, sodium chloride (NaCl), and potassium chloride (KCl) were purchased from Sinopharm

Chemical Reagent Co., Ltd. (Shanghai, China); agar powder ( $(C_{12}H_{18}O_9)_n$ ), ethylenediaminetetraacetic acid disodium salt (EDTA-2Na,  $C_{10}H_{14}N_2Na_2O_8$ ), sodium dodecyl sulfate (SDS,  $C_{12}H_{25}SO_4Na$ ), triton X-100 ( $C_{34}H_{62}O_{11}$ ), kanamycin sulfate, ampicillin sodium, crystal violet ( $C_{25}H_{30}ClN_3$ ), propidium iodide (PI) solution, thiazolyl blue tetrazolium bromide (MTT), 2-(4-amidinophenyl)-6-indolecarbamidine dihydrochloride (DAPI), 10× DNA loading buffer, and Calcein-AM/PI live/dead cell dual staining kit were purchased from Beijing Solarbio Science & Technology Co., Ltd. (Beijing, China); a bacterial genomic DNA extraction kit was purchased from TIANGEN Biochemical Technology Co., Ltd. (Beijing, China); a 2 kb DNA ladder (100–2000 bp) was purchased from Baiolaibo Technology Co., Ltd. (Beijing, China); anti-TNF- $\alpha$  (D2D4) XP rabbit monoclonal antibody was purchased from Cell Signaling Technology; anti-IL-6 antibody (ab233706) and goat antirabbit IgG H&L (ab150078, Alexa Fluor 555) were purchased from Abcam. All mice were purchased from Jinan Pengyue Experimental Animal Breeding Co., Ltd. (Jinan, China) and were kept in a specific pathogen-free environment.

## 2.2. Synthesis and Structural Parameter Characterization of AMPs.

**2.2.1. Synthesis of AMPs.** The AMPs mentioned above were synthesized by GL Biochem (Shanghai, China) using the standard solid-phase Fmoc method, 5-carboxyltetramethyl rhodamine (TMR) fluorescein-modified 1–4 (TMR-1–4) was synthesized by Bioengineering Co., Ltd. (Shanghai, China), and the C-terminus of the AMPs was amidated. All synthesized AMPs were purified using high-performance liquid chromatography with a purity of over 95%, and their molecular weights were confirmed using mass spectrometry (MS). All AMP samples were stored at  $-20\text{ }^\circ\text{C}$ .

**2.2.2. Prediction of AMPs' Structural Parameters.** The molecular weights of all AMPs were calculated using ProtParam (<https://web.expasy.org/protparam/>). Peptide net charge and hydrophobic content were calculated using the prediction tool of the Antimicrobial Peptide Database (APD) (<https://aps.unmc.edu/prediction>). The three-dimensional (3D) structure modeling of the AMPs was performed using the 3D structure prediction website (<https://zhanglab.cmb.med.umich.edu/>). The helical wheel projection of the AMPs was calculated using the online program NetWheels: Peptides Helical Wheel and the Net projection maker (<http://lbqp.unb.br/NetWheels/>).

**2.2.3. Circular Dichroism Spectroscopy Detection of AMPs.** The secondary structures of the AMPs were probed using a circular dichroism (CD) spectrometer (Jasco J-1500, Tokyo, Japan). PBS (100 mM, pH = 7.4) was used to simulate a normal physiological environment, 50% TFE was used to simulate a hydrophobic environment, SDS (30 mM) solution was used to simulate a microbial membrane environment, and the four AMPs were dissolved in the three solvents, with a final volume of 1 mL and a final concentration of 200  $\mu\text{g/mL}$ . The CD spectra of the AMPs were measured in a 1 mm path-length quartz cell using a CD spectrometer (Jasco J-1500, Tokyo, Japan). Scanning was repeated thrice, and peak plots were generated using GraphPad Prism 7.

## 2.3. In Vitro Antimicrobial Activity and Stability Assay.

**2.3.1. Bacterial Cultivation.** Three MDR bacteria, including MDR-*Escherichia coli* (LZ-7), MDR-A. *baumannii* (AB-29), and MDR-*Enterococcus faecalis* and six pathogenic bacteria, such as *E. coli* (ATCC 25922), *Vibrio anguillarum*, *Micrococcus luteus*, *Pseudomonas adaceae* (CICC 21958),

*Listeria monocytogenes* (CICC 21529), and *Vibrio parahaemolyticus* (ATCC 17802) were used in this experiment. *V. parahaemolyticus* and *P. adaceae* were cultured in NB and BHI, respectively, whereas the rest were cultured in Luria–Bertani (LB) medium. Single bacterial colonies were cultured at  $37\text{ }^\circ\text{C}$  and 180 rpm for 12 h until the logarithmic growth phase for standby.

**2.3.2. In Vitro Antimicrobial Activity Assay.** The bacteria mentioned above were cultured to the logarithmic growth period in a medium at  $37\text{ }^\circ\text{C}$  at 180 rpm, and the bacterial density was adjusted to  $10^5\text{ cfu/mL}$  with LB for use. The minimal inhibitory concentration (MIC) was the lowest drug concentration that completely limits bacterial growth, and the MIC values of the AMPs were determined using the microbroth dilution method with slight modifications.<sup>41,42</sup> The bacterial suspensions mixed with gradient concentrations (0.5–8  $\mu\text{g/mL}$ ) of AMPs were added to a 96-well plate and placed at  $37\text{ }^\circ\text{C}$  for 18 h, during which the absorbance at 600 nm was measured hourly using a microplate reader (Thermo Fisher Scientific, Multiskan MK3, China). Growth curves were plotted using GraphPad Prism 7.

Minimal bactericidal concentration (MBC) is the lowest drug concentration that kills bacteria and was determined using the colony-count assay.<sup>23,43</sup> The bacterial suspensions ( $10^5\text{ cfu/mL}$ , 50  $\mu\text{L}$ ) were mixed with PBS, 6  $\mu\text{g/mL}$  ampicillin (Amcill-s) and kanamycin sulfate (Kana-s) solution, or gradient concentrations (2–6  $\mu\text{g/mL}$ ) of AMPs (50  $\mu\text{L}$ ) and cocultured for 30 min. After that, the bacteria were inoculated onto a solid medium, and the MBC was determined by the number of bacterial colonies formed on the solid medium. A survival rate histogram was constructed using GraphPad Prism 7.

## 2.3.3. Inhibition of Bacterial Biofilm Formation In Vitro.

Crystal violet staining was used to evaluate the inhibitory effects of antimicrobial peptides on bacterial biofilm growth.<sup>44</sup> Suspensions of *E. coli* and MDR-*E. coli* ( $10^8\text{ cfu/mL}$ ) were added to 24-well plates (1 mL per well) and cultured at  $37\text{ }^\circ\text{C}$  for 12 h. After that, the supernatant in each well was gently aspirated off, and the bacteria at the bottom of the wells were washed twice with PBS and then exposed to LB medium containing AMPs (48  $\mu\text{g/mL}$ ), either with Amcill-s (48  $\mu\text{g/mL}$ ) or Kana-s (48  $\mu\text{g/mL}$ ), and blank LB medium at  $37\text{ }^\circ\text{C}$  for 48 h. Then the supernatant was removed, and the biofilm was washed twice with PBS and fixed with methanol at  $4\text{ }^\circ\text{C}$  for 20 min. Finally, methanol was removed and fully washed, and a 0.1% crystal violet dye solution was used for dyeing for 30 min. After the dye solution was removed and washed completely, the dyeing results were photographed and recorded. At the same time, anhydrous ethanol was added into the pores to fully wash out the crystal violet in the cells, and the supernatant was added to 96-well plates. The absorbance at 550 nm was measured using a microplate reader (Thermo Fisher Scientific, Multiskan MK3, China). A biofilm quality histogram was created using GraphPad Prism 7.

## 2.3.4. Destruction of Bacterial Biofilm In Vitro.

Dead/live staining was used to assess the disruption and killing of bacterial biofilms by the AMPs, and confocal microscopy was used to visualize the 3D structures of the biofilms.<sup>45</sup> Suspensions of *E. coli* and MDR-*E. coli* ( $10^8\text{ cfu/mL}$ ) were added into confocal dishes (1 mL per dish) and cultured at  $37\text{ }^\circ\text{C}$  for 7 days, during which the solution was changed every 12 h. After aspirating the culture fluid and washing, the biofilms were exposed to the four AMPs (48  $\mu\text{g/mL}$ ) or PBS, Amcill-s

(48  $\mu\text{g}/\text{mL}$ ), or Kana-s (48  $\mu\text{g}/\text{mL}$ ) as the control group. After 2 h, bacterial biofilms were stained using a Calcein-AM/PI live/dead double staining kit (Solarbio, CA1630). After washing thrice, the stained bacterial biofilms were visualized using a confocal fluorescence microscope (Nikon, ECLIPSE Ti2-E, Japan).

**2.3.5. In Vitro Physiological Stability Assay.** Four AMPs were dissolved in PBS and incubated at 37 °C for 2, 6, 12, and 24 h at 180 rpm. The AMP solutions (MBC, 50  $\mu\text{L}$ ) were incubated for different times, and the nonincubated ones were mixed with the bacterial suspension (50  $\mu\text{L}$ ) to determine their MBC values using the method described above. The stability of the AMPs was determined by comparing the changes in their antimicrobial activity at different incubation times.

## 2.4. In Vitro Antimicrobial Mechanism of AMPs.

**2.4.1. Morphological Observation of Bacterial Cell Membrane.** Bacterial suspensions of *L. monocytogenes* and *M. luteus* ( $10^8$  cfu/mL) exposed to AMPs (24  $\mu\text{g}/\text{mL}$ ) or PBS were washed three times with PBS and fixed at 4 °C for 12 h with 2.5% glutaraldehyde. Next, 10  $\mu\text{L}$  of *L. monocytogenes* sample was dropped onto a copper mesh to cover the surface and left to stand for 10 min. The excess liquid on the copper grid was blotted away using filter paper, and the bacterial morphology was observed using transmission electron microscopy (TEM; JEOL, JSM-840) after drying. *M. Luteus* samples were prepared as ultrathin cell sections and observed using the TEM.

**2.4.2. Intracellular Localization of AMPs.** Suspensions of *L. monocytogenes*, *V. parahemolyticus*, *MDR-A. baumannii*, and *MDR-E. coli* ( $10^8$  cfu/mL, 1 mL) were exposed to 1–4 modified by fluorophore carboxytetramethyl rhodamine (TMR-1–4, 12  $\mu\text{g}/\text{mL}$ ) at 37 °C for 1, 10, and 30 min. Then they were stained using DAPI solution (500  $\mu\text{L}$ , 10  $\mu\text{g}/\text{mL}$ ) at room temperature for 5 min after being washed thrice with PBS. After washing, the bacterial suspensions (10  $\mu\text{L}$ ) were dropped onto glass slides and covered with coverslips for observation under a confocal fluorescence microscope (Nikon, ECLIPSE Ti2-E, Japan).

**2.4.3. Cytoplasmic Membrane Depolarization Assay.** The ability of AMPs to depolarize the bacterial plasma membrane was assessed using the fluorescent probe DiSC<sub>3-5</sub>. The nine bacteria were dispersed in 5 mM HEPES buffer (pH 7.4, containing 100 mM KCl), and the bacterial density was adjusted to  $10^8$  cfu/mL. The bacterial suspension (100  $\mu\text{L}$  per well) was added to black 96-well plates after mixing with DiSC<sub>3-5</sub> solution (0.5  $\mu\text{M}$ ) and incubated for 30 min in the dark. The four AMPs were added to the wells separately at final concentrations of 30 and 50  $\mu\text{g}/\text{mL}$ ; a bacterial sample without AMPs was used as the control. Fluorescence changes over 30 min at an excitation wavelength of 620 nm and an emission wavelength of 670 nm were detected immediately using a microplate reader (PerkinElmer, Enspire2300, USA). The fluorescence intensity–change curve was plotted using GraphPad Prism 7.

**2.4.4. Cytoplasmic Membrane Permeability Analysis.** The nine bacterial suspensions ( $10^8$  cfu/mL) were exposed to four AMPs (12  $\mu\text{g}/\text{mL}$ ) at 37 °C for 30 min. Subsequently, the bacterial samples were stained with a PI solution (10  $\mu\text{L}/\text{mL}$ , 1 mL) for 30 min in the dark after being washed extensively with PBS. The intracellular fluorescence was measured using a flow cytometer (Beckman Coulter, FC500 MPL, USA).

**2.4.5. Detection of DNA Degradation.** The nine bacterial suspensions ( $10^8$  cfu/mL, 1 mL) were treated separately with PBS or four AMPs (12  $\mu\text{g}/\text{mL}$ ) at 37 °C. After 30 min of

treatment, genomic DNA was collected using a bacterial genomic DNA extraction kit (TIANGEN, China). Genomic DNA bands were identified by agarose gel electrophoresis using Gel Red staining.

**2.4.6. Detecting Bacterial ROS.** The nine bacterial suspensions ( $10^8$  cfu/mL, 1 mL) were treated with PBS, Amcill-s (12  $\mu\text{g}/\text{mL}$ ), Kana-s (12  $\mu\text{g}/\text{mL}$ ), or the four AMPs (12  $\mu\text{g}/\text{mL}$ ) at 37 °C after being stained with DCFH-DA (10 mM) at 37 °C for 30 min. Subsequently, the bacteria were fully washed with PBS; 20  $\mu\text{L}$  of bacterial suspensions were spread on the glass slides, covered with coverslips, and observed using a confocal fluorescence microscope (Nikon, ECLIPSE Ti2-E, Japan). The bacterial samples were added into black 96-well plates after 30 min of treatment, and the fluorescence intensity at an excitation wavelength of 488 nm and an emission wavelength of 525 nm was detected immediately using a microplate reader (Thermo Fisher Scientific, Multiskan MK3, China).

**2.5. In Vivo Antimicrobial Activity Assay.** Animal experiment in the study was performed according to the international, national, and institutional rules; all applicable institutional and governmental regulations concerning the ethical use of animals were followed. Healthy 6–8 week-old female ICR mice (weighing 18–20 g) were randomly divided into six groups with six mice in each group. *MDR-A. baumannii* was dispersed in PBS, and the bacterial density was adjusted to  $2 \times 10^8$  cfu/mL. After anesthesia, the right hind limb of each mouse was injected subcutaneously with 100  $\mu\text{L}$  of the bacterial suspension to establish the bacterial skin infection model. All mice were injected subcutaneously 24 h after infection with 100  $\mu\text{L}$  of the four AMPs (200  $\mu\text{g}/\text{mL}$ ), Amcill-s (200  $\mu\text{g}/\text{mL}$ ), or PBS as a control daily for 7 consecutive days. The weight and survival of the mice were recorded within 7 days. Seven days later, all mice were euthanized and dissected. Parts of the heart, liver, spleen, lungs, kidneys, and skin tissues were fixed by immersion in a 4% formaldehyde solution to prepare paraffin sections for hematoxylin and eosin (H&E) staining; the fixed skin tissues were also Gram-stained simultaneously. All H&E and Gram-stained tissue sections were observed by a microscope (Nikon, ECLIPSE Ti2, Japan). In addition, frozen sections of the skin tissues were made by quenching in liquid nitrogen for immunofluorescence staining (IL-6 and TNF- $\alpha$ ) and were observed using fluorescence microscopy (Leica, DM4 B, Germany). Fresh heart, liver, spleen, lungs, kidneys, and skin tissues were immersed in PBS, pulverized, and homogenized. The bacteria in the tissue fluid were cultured in a solid LB medium to determine their bacterial content.

**2.6. In Vivo Biocompatibility Assay.**  
**2.6.1. Cytotoxicity Assay.** Murine macrophages RAW264.7 were cultured to the logarithmic growth phase, seeded into 96-well plates at a density of  $10^5$  cells per well, and placed in a cell incubator (5% CO<sub>2</sub>, 37 °C) for 24 h. The supernatant was removed, and DMEM medium containing various concentrations of AMPs (12, 25, 50  $\mu\text{g}/\text{mL}$ ) was added for 4 h. Samples without AMPs were used as blank control. Subsequently, 20  $\mu\text{L}$  of MTT (5 mg/mL) was added to each well after removing the supernatant and incubated for another 4 h. Finally, the supernatant from each well was removed, and 150  $\mu\text{L}$  of DMSO was added to dissolve the crystals fully. The absorbance was measured at 570 nm using a microplate reader (Thermo Fisher Scientific, Multiskan MK3, China).

The calculated survival rate histograms were plotted using GraphPad Prism 7.

**2.6.2. Hemolytic Activity Assays.** Fresh blood was collected and washed with PBS, and erythrocytes were collected until the supernatant was clear. A 2% V/V erythrocyte suspension dispersed in PBS was mixed with AMPs with a final concentrations of 2, 4, 8, 12, 24, and 48  $\mu\text{g}/\text{mL}$ . Samples with PBS only were used as the negative control, and samples with 2% Triton X-100 only were used as the positive control. After 2 h of gentle incubation at 37  $^{\circ}\text{C}$ , the supernatant was collected by centrifugation, and the absorbance of the supernatant at 570 nm was determined using a microplate reader (Thermo Fisher Scientific, Multiskan MK3, China). The hemolysis rate histogram was plotted using GraphPad Prism 7.

**2.6.3. In Vivo Hematologic Toxicity Analysis.** Healthy 6–8 week old female ICR mice, weighing 18–20 g, were selected and divided into five groups (four mice per group). Each mouse was injected daily via the tail vein with 100  $\mu\text{L}$  of the AMPs (200  $\mu\text{g}/\text{mL}$ ) or PBS for two consecutive days. Mouse blood was collected from the canthal inner canthi on the first and seventh days after injection and mixed with an anticoagulant. An automated hematology analyzer (MIND-RAY, BC-2800Vet, China) was used for hematological index detection.

**2.6.4. Drug Resistance Induction Assay.** *E. coli*, *L. monocytogenes*, and *V. parahemolyticus* were mixed with AMPs (2  $\mu\text{g}/\text{mL}$ ) in the LB and incubated at 37  $^{\circ}\text{C}$ , 180 rpm. The bacteria were passaged 12 hourly and subjected to one month of drug resistance induction. Bacteria cultured with drug resistance induction were used to detect MBC values according to the method described above.

**2.7. Statistical Analysis.** All quantified data were expressed as the mean and standard deviation (SD) and analyzed using GraphPad Prism version 5. Statistical analyses were performed using an unpaired *t*-test. Differences in the data were considered significant at \* $p < 0.05$ , \*\* $p < 0.01$ , \*\*\* $p < 0.001$ , and \*\*\*\* $p < 0.0001$ .

### 3. RESULTS

#### 3.1. Design, Synthesis, and Characterization of AMPs.

Firstly, lysine (K) was used to replace the uncharged amino acids L2, C3, and L6 in the mBjAMP1 peptide chain using computer-aided design technology to increase the net charge. Next, tryptophan (W) was used to sequentially replace the amino acids N1, A4, A8, and T11 in mBjAMP1 to improve its hydrophobicity, and ultimately 1–4 (Table 1) was obtained. Subsequently, the *S. aureus* (YSTCDFIMWKK),<sup>38</sup> *Lactobacillus monocytogenes* (ASSLLVG),<sup>39</sup> and *Pseudomonas* (KKHRKHKHH)<sup>40</sup> pheromone fragments were connected to the N-terminal of 1–4 to construct the derived hybrid peptides S-4, L-4, and P-4 (Table 1), promoting the aggregation ability of hybrid AMPs with the efficient

**Table 1. Amino Acid Sequence of the Designed AMPs**

AMPs	sequence
mBjAMP1	NLCASLRARHTIPQCKKFGRR
1–4	WKKWSKRWRHWIPQCKKFGRR
S-4	YSTCDFIMWKKWSKRWRHWIPQCKKFGRR
L-4	ASSLLVGWKKWSKRWRHWIPQCKKFGRR
P-4	KKHRKHKRHKHWKKWSKRWRHWIPQCKKFGRR

membrane affinity of bacterial pheromones and enhancing their antimicrobial activity.

The molecular weights of the AMPs were verified using MS. As shown in Table 2 and Figure S1, the relative molecular

**Table 2. Relevant Property Parameters of the Designed AMPs**

AMPs	purity (%)	M. Wt. (actual value)	M. Wt. (theoretical value)	net charge	hydrophobic ratio (%)
mBjAMP1				+6	38
1–4	96.6	2897.5	2898.5	+9	33
S-4	95.6	3858.6	3859.6	+8	37
L-4	96.8	3638.3	3639.3	+9	41
P-4	96.2	4555.4	4556.4	+17	21

masses were similar to the calculated molecular weights, and the purity exceeded 95%, indicating the successful synthesis of 1–4, S-4, L-4, and P-4. The hydrophobic ratios of the four AMPs ranged from 21 to 41%, with L-4 having the highest hydrophobic ratio. All AMPs were positively charged, with net charges ranging from +8 to +17; the P-4 had the highest net charge. The 3D structure prediction of AMPs shows that 1–4 could not mimic the  $\alpha$ -helical structure, whereas S-4, L-4, and P-4, modified by bacterial pheromones, exhibited extended helical structures (Figure 1A–C). As shown in Figure 1D, the four AMPs showed amphiphilic helical wheel structures with an even distribution of hydrophilic (red, blue, pink) and hydrophobic (green) amino acid residues on both sides of the helical wheel. Notably, S-4, L-4, and P-4, with more hydrophilic amino acids (D, C, S, H, and K) inserted between the continuously arranged hydrophobic amino acids (green), achieved the separation of the continuous hydrophobic surface and exhibited an incompletely symmetrical helical wheel structure. Moreover, the CD spectroscopy results (Figure 1E) show that the 1–4 and S-4 spectra in 10 mM PBS (pH 7.4) and 50% TFE solution<sup>46</sup> had unordered conformations without forming  $\alpha$ -helix structures. Furthermore, faint negative dichroic bands were observed at  $\sim 208$  and  $\sim 222$  nm in the L-4 and P-4 spectra, indicating  $\alpha$ -helix conformations. Similarly, the spectra of the four AMPs indicated possible  $\alpha$ -helix conformations in the presence of 30 mM anionic SDS;<sup>47</sup> however, 1–4 still did not form an  $\alpha$ -helix structure. In brief, L-4 and P-4 exhibited a more likely tendency to form  $\alpha$ -helix structures in any physiological environment.

#### 3.2. In Vitro Antimicrobial Activity and Stability of AMPs.

**3.2.1. In Vitro Antimicrobial Activity of AMPs.** The MIC and MBC values summarized in Table 3 indicate that 1–4, S-4, L-4, and P-4 have broad-spectrum antimicrobial activities against both Gram-negative and Gram-positive bacteria. At concentrations below 6  $\mu\text{g}/\text{mL}$ , they significantly inhibited the growth of more than 99.9% of the bacteria or caused bacterial death, and the minimum MBC reached 2  $\mu\text{g}/\text{mL}$  (Figure 2A–D). Nevertheless, Amcill-s and Kana-s, two widely used antibiotics, only inhibited and killed less than 20% of all bacteria at 6  $\mu\text{g}/\text{mL}$  (Figure S2). The four AMPs could effectively kill Gram-negative and Gram-positive bacteria at lower concentrations. Among them, L-4 and P-4 had the lowest MIC and MBC, signifying stronger antimicrobial activity against various common pathogenic and MDR bacteria.

**3.2.2. In Vitro Antibiofilm Activity of AMPs.** The inhibitory effects of the AMPs on bacterial biofilms at the initial stage (12

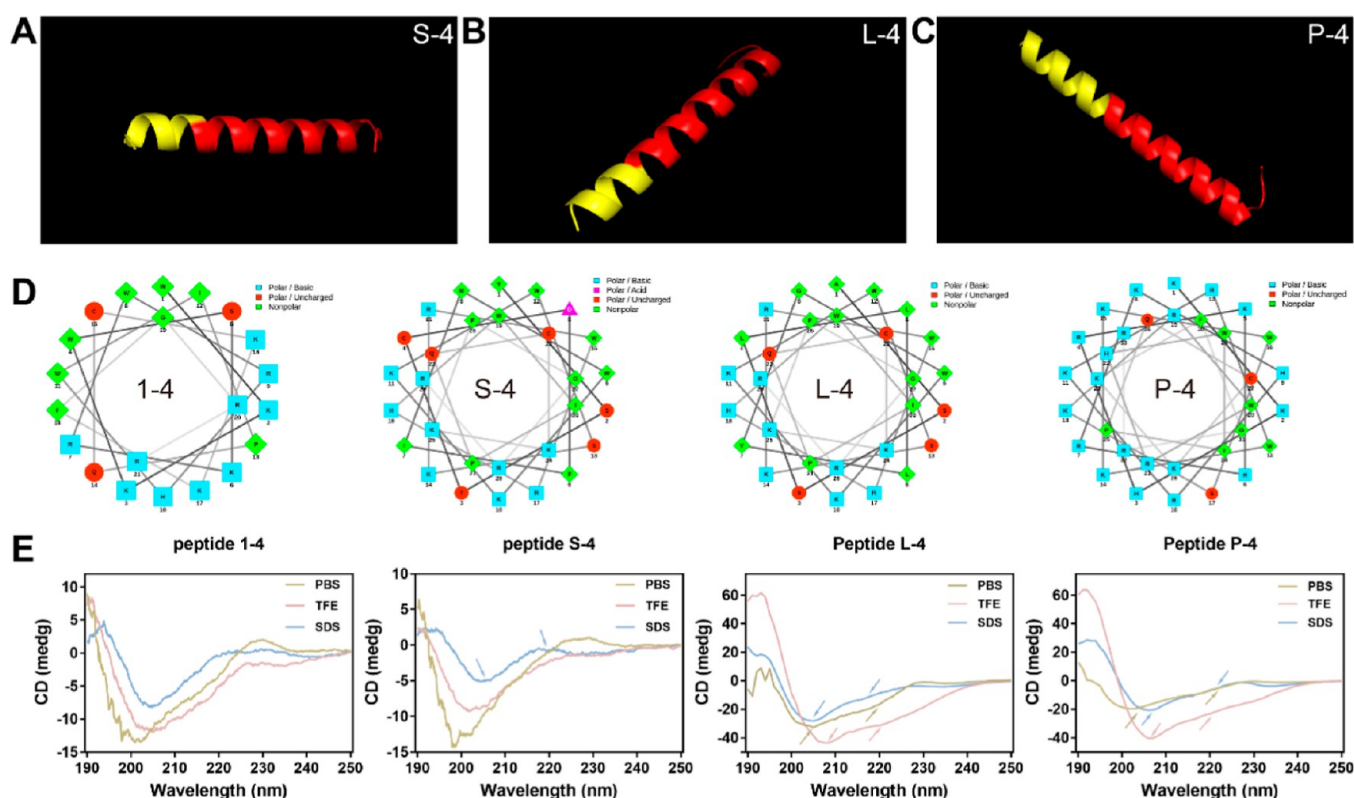


**Figure 1.** Secondary structure characterization of AMPs. 3D structural model prediction of (A) S-4, (B) L-4, and (C) P-4; the red sections represent 1–4, and the yellow sections represent the *Pseudomonas*, *S. aureus*, and *Lactobacillus monocytogenes* pheromones. (D) Helical wheel projections of 1–4, S-4, L-4, and P-4; the hydrophobic residues are presented as green diamond-shapes, the uncharged ones in the hydrophilic residues are presented as red circles, positively charged ones are presented as blue squares, and negatively charged ones are presented as pink triangles. (E) CD spectra of 1–4, S-4, L-4, and P-4; the solvents were dissolved in 10 mM PBS (pH 7.4, yellow line), 50% TFE (pink line), or 50 mM SDS (blue line).

**Table 3. MICs and MBC ( $\mu\text{g}/\text{mL}$ ) of the Four AMPs and Two Antibiotics against Nine Bacteria**

Na-me	<i>M. luteus</i>		<i>L. monocytogenes</i>		<i>P. adaceae</i>		<i>V. anguillarum</i>		<i>V. parahemolyticus</i>		<i>E. coli</i>		MDR-E. coli		MDR-A. baumannii		MDR-E. faecalis		
	MIC	MBC	MIC	MBC	MIC	MBC	MIC	MBC	MIC	MBC	MIC	MBC	MIC	MBC	MIC	MBC	MIC	MBC	
1–4	2	6	4	6	4	6	4	>6	4	6	6	6	6	4	6	6	6	6	6
S-4	2	4	4	6	4	6	1	6	4	4	4	6	6	4	2	2	6	6	6
L-4	1	4	2	4	4	4	1	6	2	2	2	4	2	4	6	6	4	4	2
P-4	1	2	2	2	2	4	1	6	2	4	2	4	2	2	6	6	4	4	4
A-s	>6	>6	>6	>6	>6	>6	>6	>6	>6	>6	>6	>6	>6	>6	>6	>6	>6	>6	>6
K-s	>6	>6	>6	>6	>6	>6	>6	>6	>6	>6	>6	>6	>6	>6	>6	>6	>6	>6	>6

h) are shown in Figure 3A. Compared with the control and antibiotic treatment groups, the membrane bands of *E. coli* and MDR-*E. coli* biofilms treated with the four AMPs for 48 h were broken; the membrane density was significantly lower than that of the control group. Moreover, the crystal violet content of the bacterial cells was significantly reduced (Figure 3B), and the biofilm mass was reduced to less than 20%. In addition, AMPs damaged the established bacterial biofilms. The green fluorescence, indicative of live bacteria, in the antibiotic treatment group was equivalent to that of the control group, and the biofilm was almost complete (Figure 3C). While the green fluorescence of the AMPs treatment group decreased significantly, the red fluorescence of the dead bacteria was enhanced. In particular, there was almost no green fluorescence signal in the L-4 and P-4 treatment groups but strong red fluorescence. In conclusion, the four AMPs

inhibited the proliferation of bacterial biofilms at the initial stage of biofilm formation and caused the destruction and dispersion of established bacterial biofilms by reducing their volume and thickness.

**3.2.3. Antimicrobial Activity Stability of AMPs.** The stability of the antimicrobial activity of AMPs (Figure 4A–F) shows that their activity against pathogenic and MDR bacteria was preserved after treatment at 37 °C for 2, 6, 12, and 24 h. The bactericidal activities of AMPs before and after treatment were similar.

**3.3. Predominant Triple Mechanism of AMPs Action.** The intracellular tracer localization results in Figures 5 and S4 show that within 1 min of binding to the bacteria, the red-fluorescent TMR-1–4 (Figure S3) was located on the surface of MDR-A. *baumannii* and MDR-E. *coli* and rapidly penetrated the cell membrane. After 10 min, the merged diagram shows

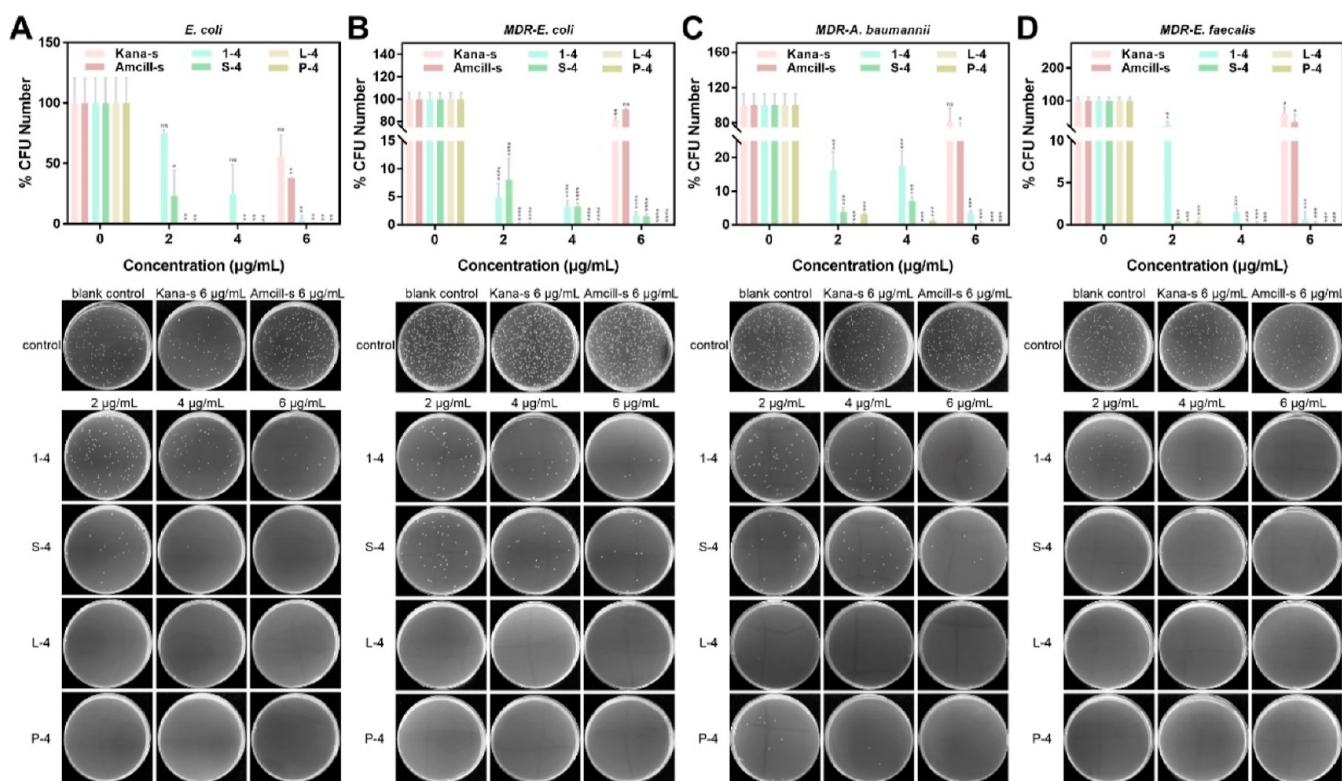


**Figure 2.** Bactericidal activity of AMPs. Survival rates and agar plates photographs of (A) *E. coli*, (B) MDR-*E. coli*, (C) MDR-*A. baumannii*, and (D) MDR-*E. faecalis* treated with 1–4, S-4, L-4, and P-4 (2, 4, 6 µg/mL) or Amcill-s or Kana-s (6 µg/mL). Data are presented as mean ± SD ( $n = 3$ ); \* means  $p < 0.05$ , \*\* means  $p < 0.01$ , \*\*\* means  $p < 0.001$ , \*\*\*\* means  $p < 0.0001$ , and ns means no significant difference.

that TMR-1–4 had entered the cells in large amounts and was partially bound to the bacterial DNA labeled by blue fluorescence. After 30 min, the pink area produced by the overlap of red and blue fluorescence increased, and the fluorescence intensity increased significantly, indicating that the AMPs could pass through the cell membrane into the cell gradually over time and accumulate on the cell membrane and DNA eventually.

TEM was used to observe morphological changes and cell membrane damage caused by AMPs. Figure 6A shows that the bacteria in the control group were full and smooth, with a clear and complete bilayer membrane structure and dense cytoplasm. While the bacterial membranes were rough and ruptured, the boundaries of the bilayer membranes were blurred, and the intracellular contents leaked after treatment with 1–4, S-4, L-4, and P-4, particularly L-4 and P-4. Simultaneously, the ultrathin cell section in Figure 6B indicates that after treatment with AMPs, particularly L-4 and P-4, the morphology of the bacterial cell membrane became wrinkled and warped. This led to decreased density of the cell contents, indicating the leakage of intracellular contents.

To explain the antimicrobial mechanisms leading to membrane breakage, we characterized the physicochemical properties of the bacterial membranes. Cell membrane depolarization (Figures 6C–F, S5) shows that there was a rapid and similar increase in the relative fluorescence intensity induced by the addition of the four AMPs compared with the control group; the depolarization effect of L-4 and P-4 was more significant. In addition, the cell membrane permeability results (Figures 6G–J, S6) show that more than 85% of the cells in the control group presented no PI fluorescence signal, indicating that the cell membranes were intact. However, more

than 50% of the bacteria in the 1–4, S-4, L-4, and P-4 treatment groups were stained with PI, suggesting increased cell membrane permeability with the four AMPs.

Moreover, the degradation evaluation of bacterial genomic DNA (Figures 7A and S7A) shows that the brightness of the DNA bands was significantly reduced after AMPs treatment than before, implying DNA degradation. Furthermore, the level of intracellular ROS was evaluated using the ROS-sensitive fluorescent probe DCFH-DA.<sup>48,49</sup> According to the intracellular fluorescence intensity in Figures 7B,C, S7B–I, and S8, treatment with AMPs resulted in evident green fluorescence of ROS in the bacteria, and the fluorescence intensity was significantly higher than that of the control, Kana-s, and Amcill-s groups. Moreover, the levels of intracellular ROS suggested that the enhanced antibacterial activity of AMPs, such as L-4 and P-4, could increase ROS production.

**3.4. In Vivo Anti-inflammatory Effect Evaluation of AMPs.** Mice with skin infected with MDR-*A. baumannii* were treated with 1–4, S-4, L-4, and P-4. It can be observed from images of the skin during treatment (Figure 8A) that the infection of the control mice progressed rapidly, with skin ulcerations and open wounds forming within 7 days. Subcutaneous injection of the Amcill-s in situ did not accelerate the healing of the skin lesions, and a prominent pustular crust remained on the infected skin after 7 days of administration. Whereas, injection of 1–4, S-4, L-4, and P-4 significantly delayed the formation of inflammation and accelerated the skin's self-healing process. Among them, L-4 and P-4 showed the most outstanding therapeutic effects, and the skin was almost intact after treatment, consistent with their antimicrobial effects in vitro. This finding indicates that they could maintain good antimicrobial ability in vivo. In addition,

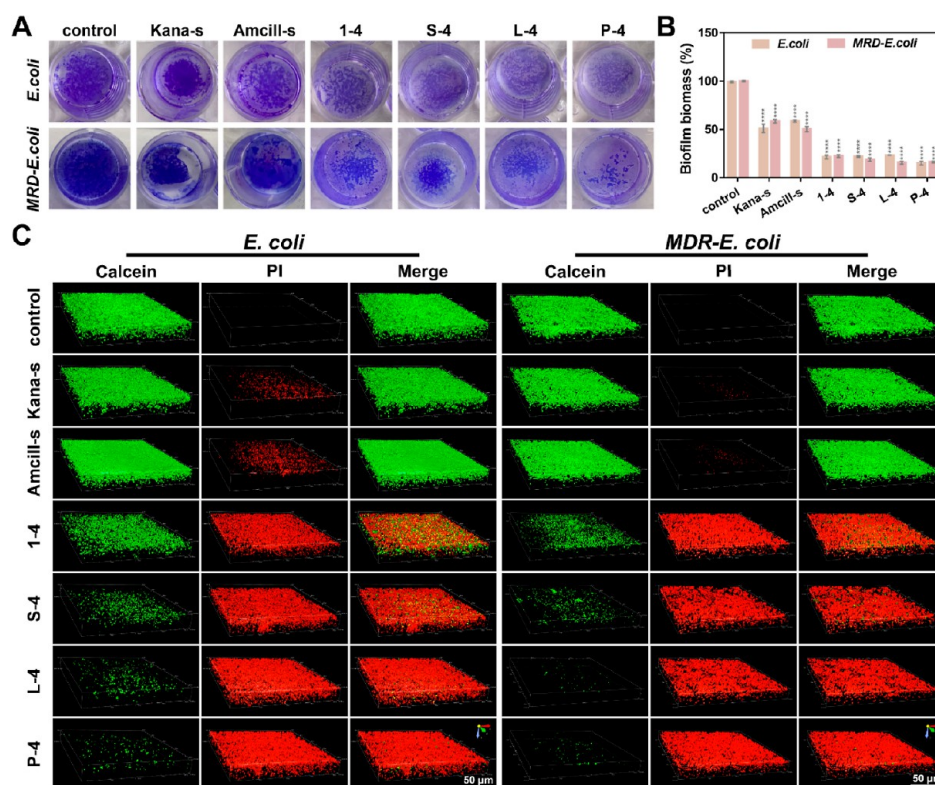


**Figure 3.** Antibiofilm activity of AMPs. (A) Photographs and (B) membrane quality quantification of crystal violet stained *E. coli* and MDR-*E. coli* biofilms treated with 1-4, S-4, L-4, and P-4 (48  $\mu\text{g}/\text{mL}$ ) or Amcill-s or Kana-s (48  $\mu\text{g}/\text{mL}$ ). Data are presented as mean  $\pm$  SD ( $n = 3$ ); \*\*\*\* means  $p < 0.0001$ . (C) Confocal images of Calcein-AM/PI-stained *E. coli* and MDR-*E. coli* biofilms treated with 1-4, S-4, L-4, and P-4 (48  $\mu\text{g}/\text{mL}$ ) or Amcill-s or Kana-s (48  $\mu\text{g}/\text{mL}$ ). (Red: PI, excitation wavelength is 535 nm, emission wavelength is 615 nm; Green: Calcein, excitation wavelength 494 nm, emission wavelength 514 nm). Scale bar: 50  $\mu\text{m}$ .

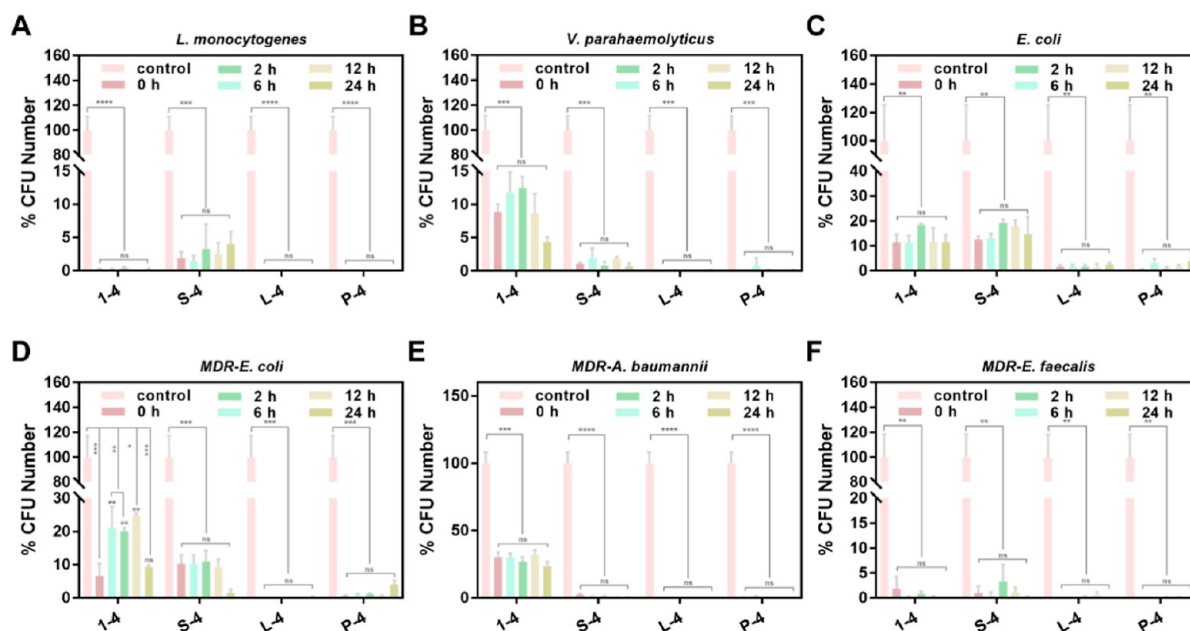


**Figure 4.** Stability of the antimicrobial activity of AMPs. Survival rates of (A) *L. monocytogenes*, (B) *V. parahemolyticus*, (C) *E. coli*, (D) MDR-*E. coli*, (E) MDR-*A. baumannii*, and (F) MDR-*E. faecalis* treated with 1-4, S-4, L-4, and P-4, which were pre-treated at 37  $^{\circ}\text{C}$  for different time (0, 2, 4, 6, 12, and 24 h). Data are presented as mean  $\pm$  SD ( $n = 3$ ); \* means  $p < 0.05$ , \*\* means  $p < 0.01$ , \*\*\* means  $p < 0.001$ , \*\*\*\* means  $p < 0.0001$ , and ns means no significant difference.

the bacterial count in the infected site (Figure 8B) shows that 1-4, S-4, L-4, and P-4 could effectively eliminate the bacteria at the inflammatory site, and the bacterial mortality reached

over 98%, much higher than that in the PBS and Amcill-s groups. Figure S9A–D reveals that MDR-*A. baumannii* infection had spread from the skin to the main organs.

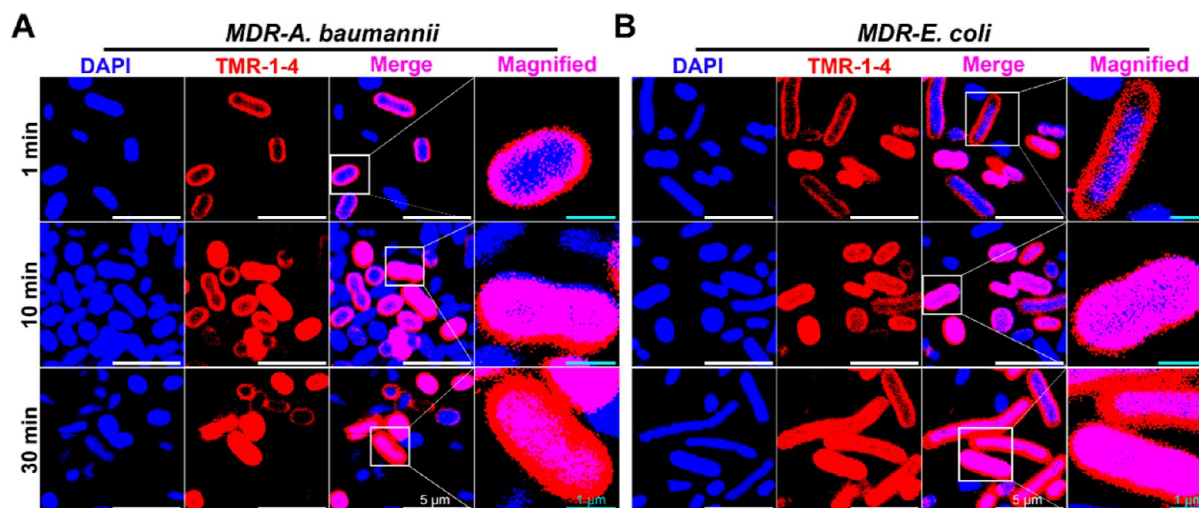


**Figure 5.** Colocalization of AMPs with bacteria. Intracellular fluorescence images of DAPI-stained (A) MDR-*A. baumannii* and (B) MDR-*E. coli* treated with TMR-1–4 (12  $\mu\text{g}/\text{mL}$ ) for 1, 10, and 30 min (Red: TMR-1–4, excitation wavelength 558 nm, emission wavelength 586 nm; Blue: DAPI, indicating nuclei, excitation at 340 nm and emission at 488 nm; Pink: Merge, the overlap of red fluorescence and blue fluorescence). White scale bar: 5  $\mu\text{m}$ , green scale bar: 1  $\mu\text{m}$ .

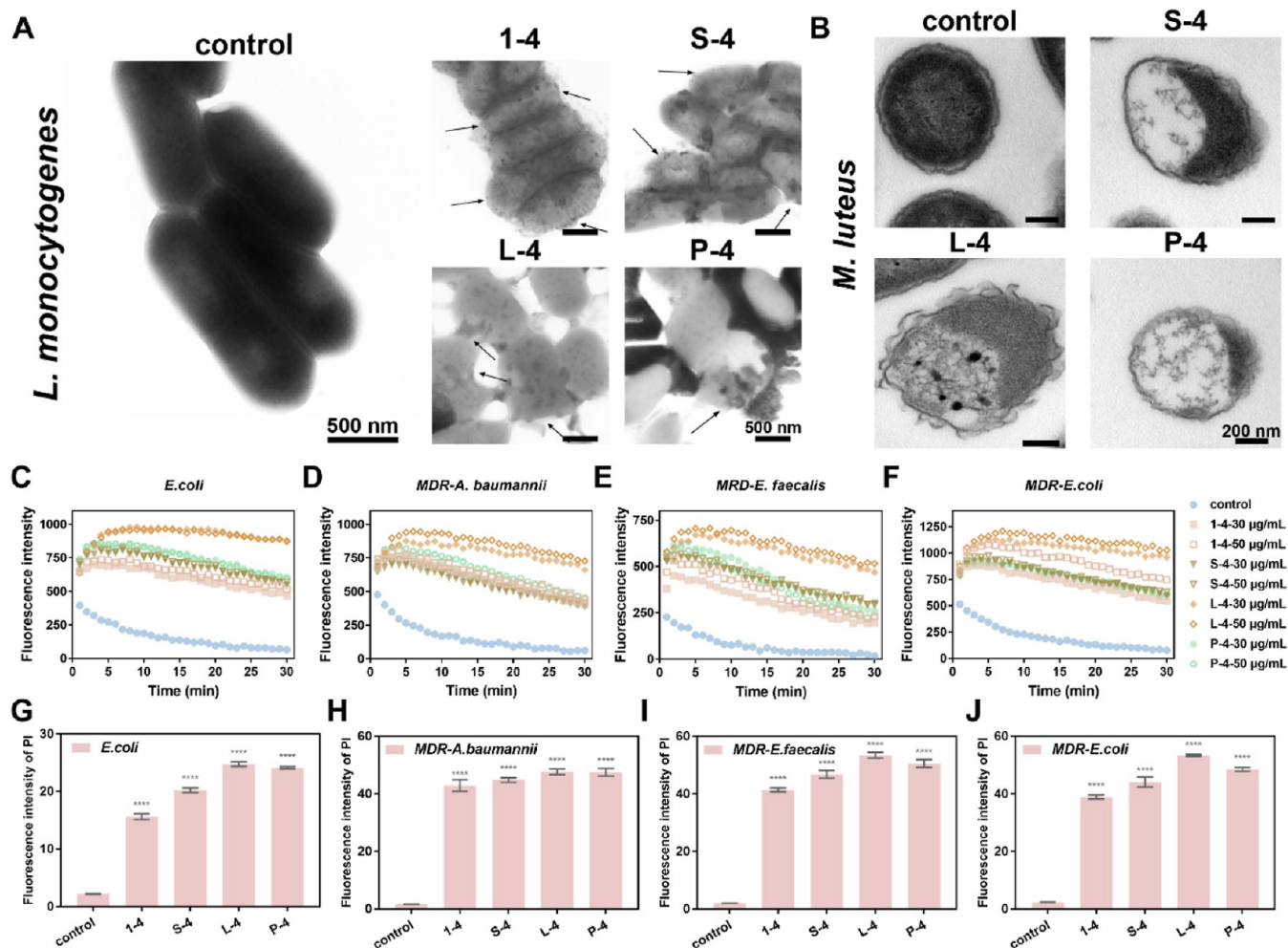


**Figure 6.** Membrane disruption mechanism of AMPs. (A) TEM micrographs of *L. monocytogenes* untreated and treated with 1–4, S-4, L-4, and P-4 (24  $\mu\text{g}/\text{mL}$ ); scale bar: 500 nm. (B) TEM micrographs of *M. luteus* ultrathin section untreated and treated with S-4, L-4, and P-4 (24  $\mu\text{g}/\text{mL}$ ); scale bar: 200 nm. Cytoplasmic membrane potential variation of (C) *E. coli*, (D) MDR-*A. baumannii*, (E) MDR-*E. faecalis*, and (F) MDR-*E. coli* untreated and treated by 1–4, S-4, L-4, and P-4 (30, 50  $\mu\text{g}/\text{mL}$ ). (Excitation wavelength 622 nm, emission wavelength 670 nm). Membrane damage of (G) *E. coli*, (H) MDR-*A. baumannii*, (I) MDR-*E. faecalis*, and (J) MDR-*E. coli* untreated and treated with 1–4, S-4, L-4, and P-4 (12  $\mu\text{g}/\text{mL}$ ). (Excitation wavelength 535 nm, emission wavelength 615 nm). Data are presented as mean  $\pm$  SD ( $n = 3$ ); \*\*\*\* means  $p < 0.0001$ .

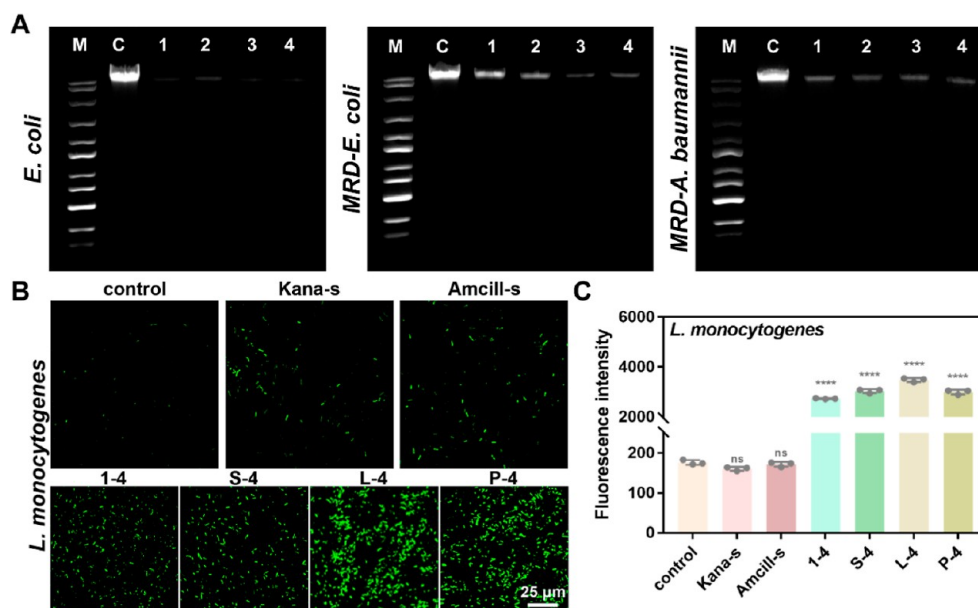


**Figure 7.** DNA and oxidative damage mechanisms of AMPs. (A) Genomic DNA degradation detection of *E. coli*, *MDR-E. coli*, and *MDR-A. baumannii* treated with 1–4, S-4, L-4, and P-4 (12 μg/mL). M, DNA Maker; C, blank control; 1, 1–4; 2, S-4; 3, L-4; 4, P-4. (B) Fluorescence images and (C) intensity quantification of *L. monocytogenes* staining by DCFH-DA after treatment with 1–4, S-4, L-4, and P-4 (12 μg/mL), Scale bar: 25 μm. Data are presented as mean ± SD ( $n = 3$ ); \*\*\*\* means  $p < 0.0001$ , ns means no significant difference.

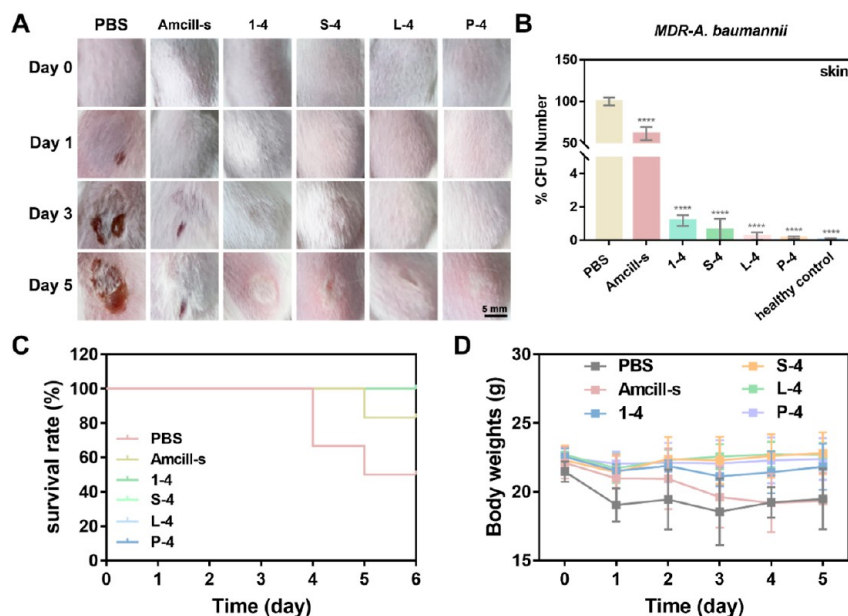


**Figure 8.** In vivo efficacy evaluation of AMPs. (A) Photographs of *MDR-A. baumannii* infected skin on treatment days 0, 1, 3, and 5 with 1–4, S-4, L-4, and P-4 (200 μg/mL). PBS as a blank control, and Amcill-s (200 μg/mL) as an antibiotic control; scale bar: 5 mm. (B) Survival rate of *MDR-A. baumannii* in inflamed skin tissue after different treatment. (C) Survival rate and (D) body weight changes of *MDR-A. baumannii* infected mice during treatment. Data are presented as mean ± SD ( $n = 3$ ); \*\*\*\* means  $p < 0.0001$ .

Additionally, leukoplakia, swelling, and histological lesions were observed in the liver and spleen of mice in PBS and Amcill-s groups. However, the bacterial loads in the liver, kidney, spleen, and lungs of the 1–4, S-4, L-4, and P-4 treatment groups were significantly reduced, and the morphological and histological characteristics of each organ were not significantly different from those of healthy mice, verifying that AMPs could maintain excellent antimicrobial activity in vivo to eliminate bacteria in infected tissues effectively.

It is reassuring that all mice in the 1–4, S-4, L-4, and P-4 groups survived and gained weight steadily during the treatment, while those mice in the PBS and Amcill-s groups lost weight and died on the fourth and fifth days of treatment, with final survival rates of 50 and 83.3%, respectively (Figure 8C,D). This finding proves that effective and safe treatment regimens of AMPs could alleviate wasting and death caused by inflammation, without side effects or other adverse reactions.

Furthermore, the H&E staining photos in Figure 9A present that the skin surface layer and dermis were intact, and the subcutaneous hair follicles and blood vessels were clear in 1–4,

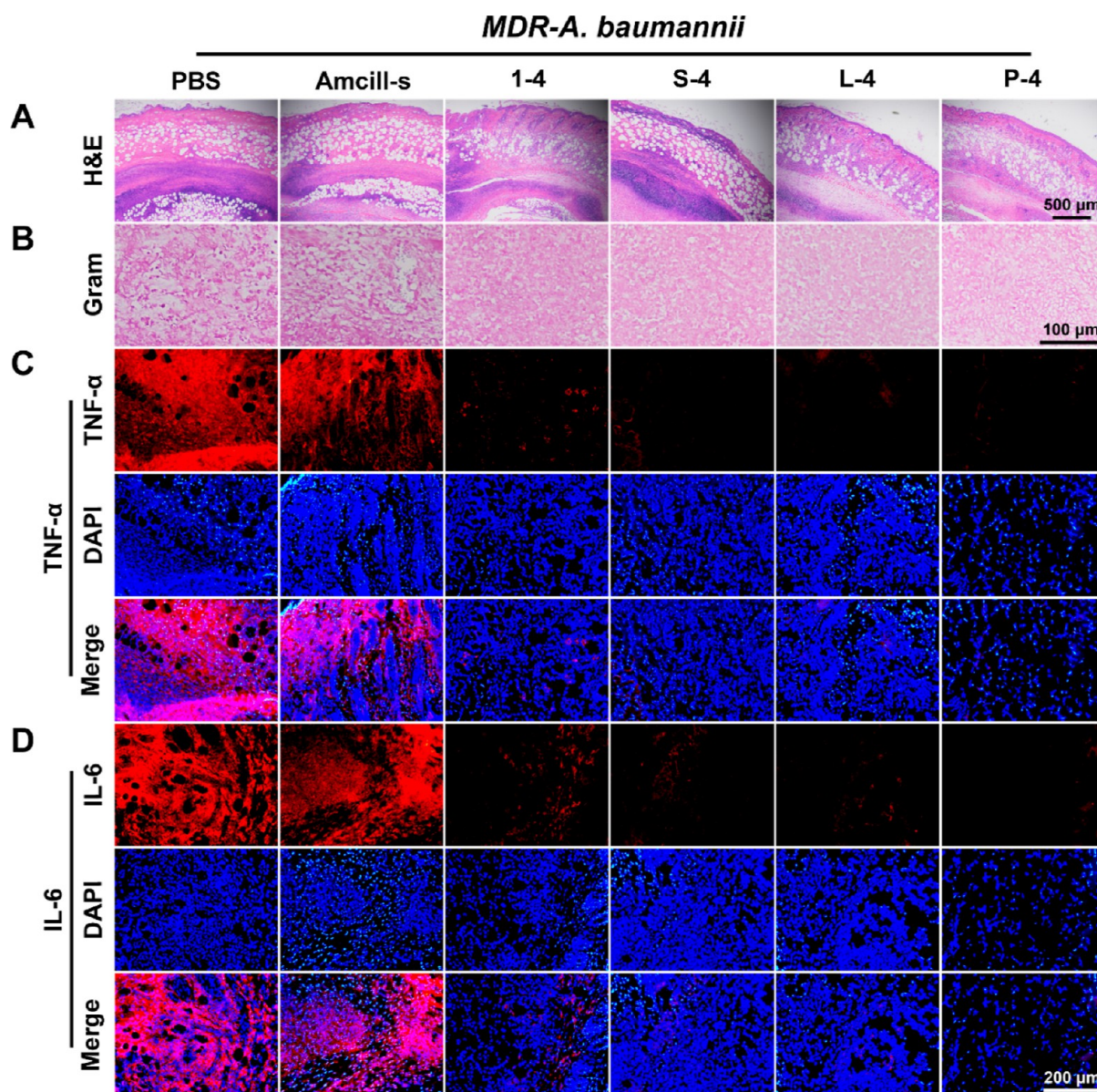


**Figure 9.** Histopathological evaluation of AMPs treatment in vivo. (A) H&E-stained images, scale bar: 500  $\mu$ m; (B) Gram-stained images, scale bar: 100  $\mu$ m; (C) immune cell marker (TNF- $\alpha$ )-stained images, and (D) immune cell marker (IL-6)-stained images of skin tissue after different treatments, scale bar: 200  $\mu$ m.

S-4, L-4, and P-4 groups. The skin was damaged, and the hair follicles and blood vessels were not formed in the PBS and Amcill-s groups. This finding indicates that the AMPs can effectively restore skin tissue damage caused by bacterial infection. More convincingly, in the Gram staining images of the skin tissue (Figure 9B), *A. baumannii*, which stained dark red, was not observed in the skin tissue of the AMPs group, which was consistent with the quantitative results of bacteria in the skin tissue. In contrast, numerous dark red *A. baumannii* were observed in the skin tissue of the PBS and Amcill-s groups, which could intuitively prove that the AMPs effectively eliminated bacteria at the infected site. Meanwhile, the immunofluorescence staining results for the pro-inflammatory factors TNF- $\alpha$  and IL-6 in the skin tissue are shown in Figure 9C and D. The red fluorescence of TNF- $\alpha$  and IL-6 in the AMPs group was significantly reduced compared to that in the PBS and Amcill-s groups, indicating that AMPs could significantly down-regulate the expression of related pro-

inflammatory genes in the bacteria-infected skin tissue and resolve inflammation.

**3.5. In Vivo Biocompatibility Evaluation of AMPs.** The results of mammalian cytotoxicity in Figure 10A–D show that there was no discernible difference in the cytotoxicity of S-4, L-4, and P-4 toward RAW264.7 cells at varying concentrations compared to the control, and the cell survival rate remained consistently high, staying above 80% and even approaching 100%. The cytotoxicity of 1–4 was marginally higher than that of the other three groups but only at the highest concentration (48  $\mu$ g/mL) did it cause a certain killing of RAW264.7 cells (mortality rate 21.7%), while the cell survival rate at lower concentrations (12, 24  $\mu$ g/mL) exceeded 90%. Although the toxicity of 1–4 was slightly higher than that of S-4, L-4, and P-4, it was evident that all four AMPs exhibited no apparent mammalian cytotoxicity within the effective MBC and MIC ranges.

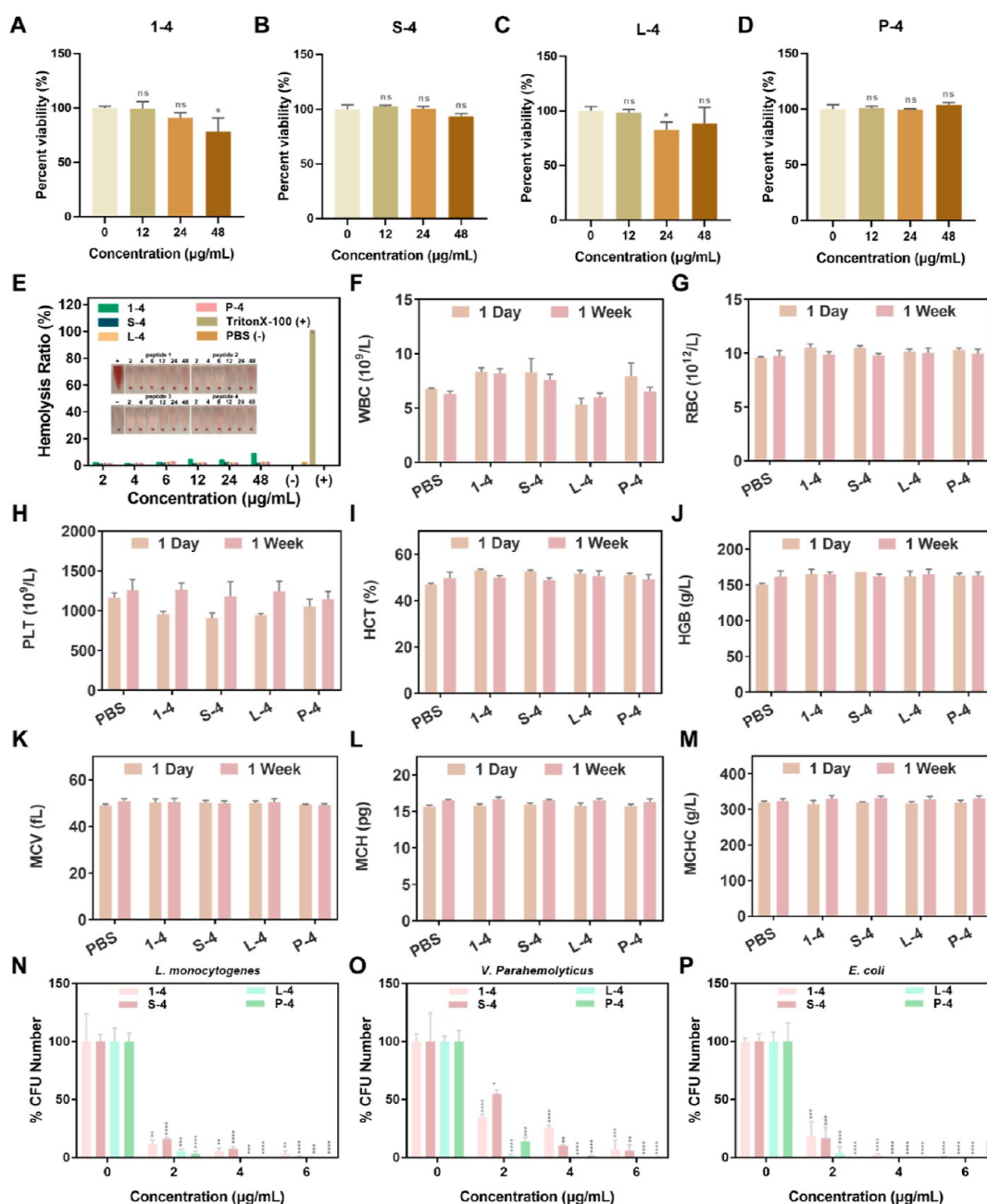


**Figure 10.** Biosafety evaluation of AMPs. Survival rate of RAW264.7 cells treated with gradient concentrations (12, 24, and 48  $\mu\text{g/mL}$ ) of (A) 1-4, (B) S-4, (C) L-4, and (D) P-4; PBS was blank control. (E) Hemolytic assays of 1-4, S-4, L-4, and P-4 with gradient concentrations (2–48  $\mu\text{g/mL}$ ); Triton X-100 was positive (+) control and PBS was negative (–) control. Hematological parameters of (F) WBC, (G) RBC, (H) PLT, (I) HCT, (J) HGB, (K) MCV, (L) MCH, and (M) MCHC in mice on days 1 and 10 after tail vein injection of 1-4, S-4, L-4, and P-4 (200  $\mu\text{g/mL}$ ). Survival rate of (N) *L. monocytogenes*, (O) *V. parahemolyticus*, and (P) *E. coli* after drug resistance induction with 1-4, S-4, L-4, and P-4 (2  $\mu\text{g/mL}$ ). Data are presented as mean  $\pm$  SD ( $n = 3$ ); \* means  $p < 0.05$ , \*\* means  $p < 0.01$ , \*\*\* means  $p < 0.001$ , \*\*\*\* means  $p < 0.0001$ , and ns means no significant difference.

At the same time, the hemolytic activity evaluation results of AMPs (Figure 10E) show that even when the concentrations of AMPs were as high as 48  $\mu\text{g/mL}$ , the supernatant photos of 1-4, S-4, L-4, and P-4 groups were as clear as those of the negative control (PBS) group, and there was no erythrocyte rupture as in the positive control (Triton X-100) group. The absorbance of the supernatant at 570 nm also showed that the hemolysis rate at different concentrations of S-4, L-4, and P-4 was similar to that of the PBS group, which remained within 4%, indicating that S-4, L-4, and P-4 did not cause erythrocyte hemolysis. Only the highest concentration (48  $\mu\text{g/mL}$ ) of 1-4

showed a hemolysis rate of more than 5% (8.54%), with slight hemolysis due to the high concentration.

Next, the hematologic toxicity of 1-4, S-4, L-4, and P-4 was evaluated in vivo. The results (Figure 10F–M) show that the white blood cell (WBC) index, red blood cell (RBC) index, hemoglobin (HGB) index, hematocrit (HCT), mean corpuscular hemoglobin (MCH), mean corpuscular volume (MCV), MCH concentration (MCHC), and platelet (PLT) were not significantly different from those of healthy mice, meaning that 1-4, S-4, L-4, and P-4 did not trigger acute and chronic

hematologic toxicity, and the side effects in mice were negligible.

It is worth noting that the four AMPs maintained the same bactericidal activity against the strains (*L. monocytogenes*, *V. parahemolyticus*, *E. coli*) after the induction of resistance (Figure 10N–P), and the MBC values against the strains before and after induction were consistent. There was no resistance to 1–4, S-4, L-4, and P-4 in the induced strains, which confirmed that 1–4, S-4, L-4, and P-4 could prevent the development of rapid bacterial resistance similar to antibiotics.

#### 4. DISCUSSION

In this study, the antimicrobial activity of AMPs was detected using MDR bacteria and common pathogens, including MDR-*A. baumannii*, MDR-*E. coli*, MDR-*E. faecalis*, *V. anguillarum*, *M. luteus*, *P. adaceae*, *L. monocytogenes*, *E. coli*, and *V. parahemolyticus*. The optimized AMPs inhibited more than 99% of bacterial proliferation at approximately 0.5–6  $\mu\text{g}/\text{mL}$  and killed more than 99% of bacteria at 2–6  $\mu\text{g}/\text{mL}$ . It is encouraging that the four AMPs showed reliable antibacterial activities against MDR-*A. baumannii*, identified as the most drug-resistant bacterium by the World Health Organization. Notably, L-4 and P-4 killed more than 99% of MDR-*A. baumannii* at concentrations as low as 4 and 2  $\mu\text{g}/\text{mL}$ , respectively. In addition, L-4 and P-4 effectively inhibited the proliferation of common pathogens, such as *M. luteus* and *V. anguillarum*, by over 99% at ng/mL. In contrast, Amcill-s and Kana-s, the primary antibiotics used in clinical treatment, showed less than 30% killing rates against MDR-*A. baumannii* at 6  $\mu\text{g}/\text{mL}$ , with no significant inhibitory effect. The effective bactericidal concentrations of 1–4, S-4, L-4, and P-4 against MDR bacteria were significantly reduced. Furthermore, in addition to the excellent antibacterial activity against planktonic MDR and common pathogens, the AMPs also could destroy the dense biofilm formed by bacteria. The four AMPs, which showed similar antibiofilm and antiplanktonic activities, inhibited biofilm formation in *E. coli* and MDR-*E. coli* by more than 80% and destroyed over 90% of the bacteria in the established biofilm, demonstrating highly effective antibacterial and antibiofilm activities. Bacterial biofilm formation is an important cause of multidrug resistance in the medical system. *E. coli* can easily form a biofilm structure, but Amcill-s and Kana-s lack antibiofilm activity and can not effectively remove the biofilms of *E. coli* and MDR-*E. coli* at low concentrations. 1–4, S-4, L-4, and P-4 can achieve the inhibition and mortality of sensitive and resistant strains and their biofilms at low concentrations (0.5–6  $\mu\text{g}/\text{mL}$ ); the bactericidal dose is significantly reduced, showing a superior antibacterial effect. Moreover, the antibacterial activities of 1–4, S-4, L-4, and P-4 were preserved under simulated physiological conditions, indicating their good in vitro stability.

But in fact, there were apparent differences in the antibacterial activities of the four AMPs. Based on the MIC and MBC values, the antibacterial activities of S-4, L-4, and P-4 were higher than those of 1–4. L-4, and P-4 and showed the strongest antibacterial activity, related to changes in their secondary structure, such as positive charge, hydrophobicity, and secondary structure. Lysine (K) carries a positive charge and can promote the tight binding of peptides to the negatively charged phospholipid layer of the cell membrane.<sup>32–34</sup> Moreover, we found that the four AMPs could reverse the cell membrane potential through cell membrane depolarization detection, enabling the AMPs to exhibit better antibacterial

activity. Hydrophobic tryptophan (W) enhances the affinity of the peptide to the cell membrane;<sup>35–37</sup> the modification of the bacterial pheromone<sup>30</sup> further optimizes these structural parameters, favoring antimicrobial activity. As expected, the net charge of S-4 optimized by K and W-substitution and pheromone modification (+8) was almost similar to that of 1–4 (+9); its hydrophobicity slightly increased (37%), which was responsible for the improvement in its antibacterial activity. The net charge of L-4 did not change (+9), but its hydrophobicity increased significantly (41%), improving its antibacterial activity. The solubility of P-4 improved, and the net charge number was multiplied (+17). The incomplete amphipathic structures of L-4 and P-4 could stabilize the helical structure and contribute to the improvement of their antibacterial activity,<sup>22,50,51</sup> which is responsible for the difference in the antibacterial activity of the four AMPs. In addition to these structural parameters, the secondary structures of AMPs are also closely related to their antibacterial activities. The  $\alpha$ -helical structure is a direct form of the interaction between AMPs and cell membranes. We found that 1–4 did not form a typical  $\alpha$ -helical structure, while S-4, L-4, and P-4 formed certain extended  $\alpha$ -helices after pheromone modification. Notably, the helical contents of L-4 and P-4 were slightly higher than those of 1–4 and S-4 in an anionic micellar (SDS) environment and hydrophobic TFE solution, which realized the transition from a random coil in an aqueous solution to a helical structure induced by an anisotropic environment. Moreover, the degree of change in the permeability of bacterial cell membranes induced by AMPs was consistent with their ability to form  $\alpha$ -helices. L-4 and P-4 increased the permeability of the cell membrane more than 1–4 and S-4. Furthermore, the formation of the  $\alpha$ -helix structure facilitated the interaction with the lipid surface of the cell membrane,<sup>52,53</sup> enhancing the antibacterial activity of AMPs. In conclusion, the improvement in positive charge, hydrophobicity, extended  $\alpha$ -helix structure, and incomplete symmetric amphiphilic structures after hybridization were conducive to the binding and penetration of AMPs into the cell membrane,<sup>9</sup> which contributed certainly to the enhanced antibacterial activity of AMPs.

Cell membrane perturbations (including barrel walls, carpets, toroidal pores, electroporation, and depolarization)<sup>9</sup> are defined as the primary action modes of AMPs. But interestingly, we found that the antibacterial mechanisms of 1–4, S-4, L-4, and P-4 are not limited to a single membrane damage mechanism. High-fold intracellular tracing of AMPs under a microscope was rarely performed in the current study; therefore, fluorescein was used to label the AMPs for high-definition intracellular localization. We observed that AMPs could bind to the cell membrane within 1 min, which was so rapid that 1–4, S-4, L-4, and P-4 could completely kill more than 99% of the MDR bacteria within half an hour. However, it takes more than 2–48 h for other AMPs to exert bactericidal effects.<sup>9,54</sup> This rapid transmembrane damage provides a basis for 1–4, S-4, L-4, and P-4 to enter the bacterial interior quickly and is an important guarantee for AMPs to kill bacteria rapidly. TEM images of bacterial cell membrane morphology show that 1–4, S-4, L-4, and P-4 can rapidly induce changes in cell membrane morphology. The  $\alpha$ -helical structure of AMPs allows them to be inserted into the cell membrane, which causes lethal damage to bacteria. Therefore, the rapid transmembrane damage of AMPs can be considered as the primary direct antibacterial mechanism. In addition to binding

to cell membranes, AMPs accumulate in bacterial DNA eventually, suggesting that membrane damage mechanisms are not the only means by which AMPs kill bacteria. Based on this phenomenon, we verified DNA degradation by gel electrophoresis. We found that the AMPs could complex with and degrade nucleic acid molecules after entering the cell. Membrane breakage and DNA damage may result in the leakage of cell contents as shown in TEM. In addition, we detected ROS levels in the bacteria after AMPs treatment, suggesting that AMPs could trigger the generation of a ROS storm, which would cause fatal oxidative damage to bacteria. We conclude that the excellent antibacterial activity of 1-4, S-4, L-4, and P-4 depends on their ability to rapidly penetrate and destroy the cell membrane, stimulate the production of intracellular ROS and degrade DNA (Scheme 1). This combined action of rapid transmembrane damage, DNA degradation damage, and oxidative damage is the key factor that leads to the complete death of MDR bacteria. This combined action can achieve an efficient antibacterial effect, rapidly killing more than 99% of MDR bacteria.

In addition, the *in vivo* high anti-inflammatory effects of 1-4, S-4, L-4, and P-4 were demonstrated. AMPs can effectively eliminate bacteria and biofilms in infected skin. They also showed properties of resolving inflammation by down-regulating pro-inflammatory factors such as IL-6 and TNF- $\alpha$ , which can reduce skin tissue damage and inflammatory factor disorders caused by bacterial infection, curing skin infection rapidly. This indicated that 1-4, S-4, L-4, and P-4 retained their effective antibacterial activities *in vivo*.

Considering that the potential cytotoxicity of AMPs raises a safety concern, we evaluated the biosafety of AMPs and found that they showed selective cytotoxicity to bacterial and mammalian cells and did not cause toxicity to normal somatic cells. AMPs did not cause acute or chronic hematological toxicity, RBC damage, or adverse effects on body weight, survival rate, or the main organs of mice during *in vivo* treatment, indicating excellent biocompatibility. The primary reason AMPs can reduce the cytotoxicity of mammalian cells while maintaining antibacterial activity is the difference in cell membrane charge between eukaryotic and prokaryotic cells. The extracellular membrane of prokaryotic cells contains numerous negatively charged lipids (such as cardiolipin), whereas the bilayer membrane of eukaryotic cells contains electrically neutral cholesterol.<sup>55,56</sup> This difference in membrane potential makes cationic AMPs more likely to recognize bacteria than mammalian cell membranes, preferentially bind to bacterial cell membranes, and achieve better cell selectivity. However, S-4, L-4, and P-4 showed lower mammalian cytotoxicity than 1-4 after hybridization, owing to the formation of an incomplete symmetric amphiphilic structure after pheromone modification, weakening the hydrophobic interaction of the nonpolar face and reducing the affinity with the mammalian cell membrane.<sup>22,50,51</sup> Moreover, our AMPs showed the ability to block the progression of bacterial resistance, possibly related to their triple bactericidal mechanisms. Bacteria must change their membrane structure and genetic makeup to resist AMPs, which is highly unlikely. Therefore, it is a better bactericidal way to exert antibacterial activity by multiple mechanisms, which is the best strategy to combat bacterial resistance.

The use of AMPs as therapeutic drugs has become a popular research topic in recent years. This study provides a reasonable scheme for the design and optimization of natural AMPs from

a structure perspective. In addition, the triple combination mechanisms research in this study could provide a reference for designing efficient and safe AMPs. The AMPs obtained in this study show excellent prospects for the treatment of bacterial biofilms and MDR-*A. baumannii* infection. This dual antibacterial and antibiofilm drug is also a hot spot for treating complex diseases, such as bacterial infection,<sup>57</sup> which poses a new challenge for developing new antibacterial drugs in the future.

## 5. CONCLUSIONS

In this study, mBjAMP1 was optimized by the computer-aided design of peptide structural parameters, single-factor modification, and pheromone hybridization modification. Four novel AMPs, 1-4, S-4, L-4, and P-4, with high positive charges and hydrophobic residue ratios, have been reported. The modification of pheromones promoted the formation of the  $\alpha$ -helical structure of S-4, L-4, and P-4, giving them dual antibacterial and antibiofilm activities and enabling them to rapidly kill and destroy various bacteria and their biofilms. In addition, they retained good antibacterial stability and showed potential for the treatment of skin inflammation caused by MDR-*A. baumannii* infection *in vivo*, clearing the bacteria at the infection site and effectively alleviating the inflammatory response on the basis of safety. This enhanced antibacterial activity is primarily attributed to the triple action mechanisms of AMPs: AMPs rapidly penetrate the membrane to cause irreversible membrane damage, trigger an intracellular oxidative stress response of ROS, and then bind and degrade bacterial genomic DNA, leading to the leakage of bacterial contents and bacterial death. This triple bactericidal damage endowed AMPs with high efficiency and rapid antibacterial activity, enabling them to avoid bacterial resistance. This study offered safe and effective drug candidates to address antibiotic resistance. The findings are significant for the development of alternatives to antibiotics.

## ■ ASSOCIATED CONTENT

### SI Supporting Information

The Supporting Information is available free of charge at <https://pubs.acs.org/doi/10.1021/acsomega.4c01577>.

MS of AMPs; bactericidal activity of AMPs; colocalization of AMPs with bacteria; cytoplasmic membrane potential variation results; membrane damage results; DNA and oxidative damage mechanisms of AMPs; and intracellular ROS production and some data about *in vivo* efficacy evaluation of AMPs (PDF)

## ■ AUTHOR INFORMATION

### Corresponding Authors

Pengfei Cui – *Lab of Environmental Health and Ecological Engineering, College of Marine Life Science, Ocean University of China, Qingdao 266003, China*;  [orcid.org/0000-0002-9621-4403](https://orcid.org/0000-0002-9621-4403); Email: [cuipengfei@ouc.edu.cn](mailto:cuipengfei@ouc.edu.cn)

Shaoguo Ru – *Lab of Environmental Health and Ecological Engineering, College of Marine Life Science, Ocean University of China, Qingdao 266003, China*;  [orcid.org/0000-0001-5086-3582](https://orcid.org/0000-0001-5086-3582); Email: [rusg@ouc.edu.cn](mailto:rusg@ouc.edu.cn)

### Authors

Yifan Liu – *Lab of Environmental Health and Ecological Engineering, College of Marine Life Science, Ocean University*

of China, Qingdao 266003, China; [orcid.org/0000-0001-7722-4369](https://orcid.org/0000-0001-7722-4369)

**Rong Tan** – Lab of Environmental Health and Ecological Engineering, College of Marine Life Science, Ocean University of China, Qingdao 266003, China

Complete contact information is available at:

<https://pubs.acs.org/10.1021/acsomega.4c01577>

### Author Contributions

<sup>†</sup>Y.L. and P.C. contributed equally to this work. Y.L., P.C., and S.R. designed the study. Y.L., and R.T. performed the experiments. Y.L. performed data analysis and wrote the manuscript. P.C. and S.R. revised the manuscript. All authors contributed to the manuscript and approved the final manuscript.

### Notes

The authors declare no competing financial interest.

### ACKNOWLEDGMENTS

This research was financially supported by the National Natural Science Foundation of China (31902421). The authors also thank Ocean University of China for providing funds for highly talented young researchers. We would like to thank Editage ([www.editage.cn](http://www.editage.cn)) for English language editing.

### REFERENCES

- (1) Laxminarayan, R.; Duse, A.; Wattal, C.; Zaidi, A. K. M.; Wertheim, H. F. L.; Sumpradit, N.; Vlieghe, E.; Hara, G. L.; Gould, I. M.; Goossens, H.; Greko, C.; So, A. D.; Bigdeli, M.; Tomson, G.; Woodhouse, W.; Ombaka, E.; Peralta, A. Q.; Qamar, F. N.; Mir, F.; Kariuki, S.; Bhutta, Z. A.; Coates, A.; Bergstrom, R.; Wright, G. D.; Brown, E. D.; Cars, O. Antibiotic resistance—the need for global solutions. *Lancet Infect. Dis.* **2013**, *13* (12), 1057–1098.
- (2) Li, X.; Bai, H.; Yang, Y.; Yoon, J.; Wang, S.; Zhang, X. Supramolecular antibacterial materials for combatting antibiotic resistance. *Adv. Mater.* **2019**, *31* (5), 1805092.
- (3) Song, J.; Yuan, C.; Jiao, T.; Xing, R.; Yang, M.; Adams, D. J.; Yan, X. Multifunctional antimicrobial biometallohydrogels based on amino acid coordinated self-assembly. *Small* **2020**, *16* (8), No. e1907309.
- (4) Hussain, S.; Joo, J.; Kang, J.; Kim, B.; Braun, G. B.; She, Z. G.; Kim, D.; Mann, A. P.; Molder, T.; Teesalu, T.; Carnazza, S.; Guglielmino, S.; Sailor, M. J.; Ruoslahti, E. Antibiotic-loaded nanoparticles targeted to the site of infection enhance antibacterial efficacy. *Nat. Biomed. Eng.* **2018**, *2* (2), 95–103.
- (5) Mahlapuu, M.; Bjorn, C.; Ekblom, J. Antimicrobial peptides as therapeutic agents: opportunities and challenges. *Crit. Rev. Biotechnol.* **2020**, *40* (7), 978–992.
- (6) Hamley, I. W. Small bioactive peptides for biomaterials design and therapeutics. *Chem. Rev.* **2017**, *117* (24), 14015–14041.
- (7) Tan, P.; Fu, H.; Ma, X. Design, optimization, and nanotechnology of antimicrobial peptides: From exploration to applications. *Nano Today* **2021**, *39*, 101229.
- (8) Qi, G. B.; Gao, Y. J.; Wang, L.; Wang, H. Self-assembled peptide-based nanomaterials for biomedical imaging and therapy. *Adv. Mater.* **2018**, *30* (22), No. e1703444.
- (9) Mookherjee, N.; Anderson, M. A.; Haagsman, H. P.; Davidson, D. J. Antimicrobial host defence peptides: functions and clinical potential. *Nat. Rev. Drug Discovery* **2020**, *19* (5), 311–332.
- (10) Mishra, B.; Lushnikova, T.; Golla, R. M.; Wang, X.; Wang, G. Design and surface immobilization of short anti-biofilm peptides. *Acta Biomater.* **2017**, *49*, 316–328.
- (11) Wang, G. Database-Guided Discovery of potent peptides to combat HIV-1 or superbugs. *Pharmaceuticals* **2013**, *6*, 728–758.
- (12) Rangel, K.; Lechuga, G. C.; Provance, D. W.; Morel, C. M.; De Simone, S. G. An update on the therapeutic potential of antimicrobial

peptides against acinetobacter baumannii Infections. *Pharmaceuticals* **2023**, *16* (9), 1281.

(13) Mwangi, J.; Yin, Y.; Wang, G.; Yang, M.; Li, Y.; Zhang, Z.; Lai, R. The antimicrobial peptide ZY4 combats multidrug-resistant pseudomonas aeruginosa and acinetobacter baumannii infection. *Proc. Natl. Acad. Sci. U.S.A.* **2019**, *116* (52), 26516–26522.

(14) Jayathilaka, E. H. T. T.; Rajapaksha, D. C.; Nikapitiya, C.; De Zoysa, M.; Whang, I. Antimicrobial and anti-Biofilm peptide Octominin for controlling multidrug-resistant acinetobacter baumannii. *Int. J. Mol. Sci.* **2021**, *22* (10), 5353.

(15) Peng, J.; Wang, Y.; Wu, Z.; Mao, C.; Li, L.; Cao, H.; Qiu, Z.; Guo, G.; Liang, G.; Shen, F. Antimicrobial peptide Cec4 eradicates multidrug-resistant acinetobacter baumannii in vitro and in vivo. *Drug Des. Dev. Ther.* **2023**, *17*, 977–992. eCollection2023

(16) Cardoso, M. H.; Ribeiro, S. M.; Nolasco, D. O.; de la Fuente-Núñez, C.; Felício, M. R.; Gonçalves, S.; Matos, C. O.; Liao, L. M.; Santos, N. C.; Hancock, R. E. W.; Franco, O. L.; Migliolo, L. A polyaniline peptide derived from polar fish with anti-infectious activities. *Sci. Rep.* **2016**, *6* (1), 21385.

(17) Cardoso, M. H.; Cândido, E. S.; Chan, L. Y.; Der Torossian Torres, M.; Oshiro, K. G. N.; Rezende, S. B.; Porto, W. F.; Lu, T. K.; de la Fuente-Nunez, C.; Craik, D. J.; Franco, O. L. A Computationally designed peptide derived from Escherichia coli as a potential drug template for antibacterial and antibiofilm therapies. *ACS Infect. Dis.* **2018**, *4* (12), 1727–1736.

(18) Fjell, C. D.; Hiss, J. A.; Hancock, R. E. W.; Schneider, G. Designing antimicrobial peptides: form follows function. *Nat. Rev. Drug Discovery* **2012**, *11* (1), 37–51.

(19) Sullivan, R.; Santarpia, P.; Lavender, S.; Gittins, E.; Liu, Z.; Anderson, M. H.; He, J.; Shi, W.; Eckert, R. Clinical efficacy of a specifically targeted antimicrobial peptide mouth rinse: targeted elimination of Streptococcus mutans and prevention of demineralization. *Caries Res.* **2011**, *45* (5), 415–428.

(20) Tan, P.; Tang, Q.; Xu, S.; Zhang, Y.; Fu, H.; Ma, X. Designing self-assembling chimeric peptide nanoparticles with high stability for combating piglet bacterial infections. *Adv. Sci.* **2022**, *9* (14), No. e2105955.

(21) Lai, Z.; Jian, Q.; Li, G.; Shao, C.; Zhu, Y.; Yuan, X.; Chen, H.; Shan, A. Self-assembling peptide dendron nanoparticles with high stability and a multimodal antimicrobial mechanism of action. *ACS Nano* **2021**, *15* (10), 15824–15840.

(22) Mourtada, R.; Herce, H. D.; Yin, D. J.; Moroco, J. A.; Wales, T. E.; Engen, J. R.; Walensky, L. D. Design of stapled antimicrobial peptides that are stable, nontoxic and kill antibiotic-resistant bacteria in mice. *Nat. Biotechnol.* **2019**, *37* (10), 1186–1197.

(23) Lei, R.; Hou, J.; Chen, Q.; Yuan, W.; Cheng, B.; Sun, Y.; Jin, Y.; Ge, L.; Ben-Sasson, S. A.; Chen, J.; Wang, H.; Lu, W.; Fang, X. Self-assembling myristoylated human  $\alpha$ -defensin 5 as a next-generation nanobiotics potentiates therapeutic efficacy in bacterial infection. *ACS Nano* **2018**, *12* (6), 5284–5296.

(24) Luo, Y.; Song, Y. Mechanism of antimicrobial peptides: antimicrobial, anti-inflammatory and antibiofilm activities. *Int. J. Mol. Sci.* **2021**, *22*, 11401.

(25) Sousa, D.; Porto, W.; Silva, M.; da Silva, T.; Franco, O. Influence of cysteine and tryptophan substitution on DNA-binding activity on maize  $\alpha$ -hairpinin antimicrobial peptide. *Molecules* **2016**, *21* (8), 1062.

(26) Ramamourthy, G.; Park, J.; Seo, C.; J Vogel, H.; Park, Y. Antifungal and antibiofilm activities and the mechanism of action of repeating lysine-tryptophan peptides against candida albicans. *Microorganisms* **2020**, *8* (5), 758.

(27) Han, X.; Kou, Z.; Jiang, F.; Sun, X.; Shang, D. Interactions of designed trp-containing antimicrobial peptides with DNA of multidrug-resistant pseudomonas aeruginosa. *DNA Cell Biol.* **2021**, *40*, 414–424.

(28) He, S. w.; Wang, G. H.; Yue, B.; Zhou, S.; Zhang, M. TO17: A teleost antimicrobial peptide that induces degradation of bacterial nucleic acids and inhibits bacterial infection in red drum, Sciaenops ocellatus. *Fish Shellfish Immunol.* **2018**, *72*, 639–645.

- (29) Li, Y.; Smith, C.; Wu, H.; Teng, P.; Shi, Y.; Padhee, S.; Jones, T.; Nguyen, A.-M.; Cao, C.; Yin, H.; Cai, J. Short antimicrobial lipopeptide- $\alpha/\gamma$ -AA hybrid peptides. *ChemBioChem* **2014**, *15* (15), 2275–2280.
- (30) Lyon, G. J.; Novick, R. P. Peptide signaling in *Staphylococcus aureus* and other Gram-positive bacteria. *Peptides* **2004**, *25* (9), 1389–1403.
- (31) Liu, H.; Lei, M.; Du, X.; Cui, P.; Zhang, S. Identification of a novel antimicrobial peptide from amphioxus *Branchiostoma japonicum* by in silico and functional analyses. *Sci. Rep.* **2015**, *5*, 18355.
- (32) Avitabile, C.; Netti, F.; Orefice, G.; Palmieri, M.; Nocerino, N.; Malgieri, G.; D'Andrea, L. D.; Capparelli, R.; Fattorusso, R.; Romanelli, A. Design, structural and functional characterization of a Temporin-1b analog active against Gram-negative bacteria. *Biochim. Biophys. Acta* **2013**, *1830* (6), 3767–3775.
- (33) Strandberg, E.; Killian, J. A. Snorkeling of lysine side chains in transmembrane helices: how easy can it get? *FEBS Lett.* **2003**, *544* (1–3), 69–73.
- (34) Lu, Y.; Zou, W.; Wang, L.; Xi, X.; Ma, C.; Chen, X.; Chen, T.; Shaw, C.; Zhang, X.; Zhou, M. Kassporin-KS1: A novel pentadecapeptide from the skin secretion of *kassina senegalensis*: studies on the structure-activity relationships of site-specific "Glycine-Lysine" motif insertions. *Antibiotics* **2022**, *11* (2), 243.
- (35) Kang, S. J.; Won, H. S.; Choi, W. S.; Lee, B. J. De novo generation of antimicrobial LK peptides with a single tryptophan at the critical amphipathic interface. *J. Pept. Sci.* **2009**, *15* (9), 583–588.
- (36) Ridder, A. N. J. A.; Morein, S.; Stam, J. G.; Kuhn, A.; de Kruijff, B.; Killian, J. A. Analysis of the role of interfacial tryptophan residues in controlling the topology of membrane proteins. *Biochemistry* **2000**, *39* (21), 6521–6528.
- (37) Hu, W.; Lee, K. C.; Cross, T. A. Tryptophans in membrane proteins: Indole ring orientations and functional implications in the gramicidin channel. *Biochemistry* **1993**, *32* (27), 7035–7047.
- (38) Dunny, G. M.; Leonard, B. A. B. Cell-cell communication in gram-positive bacteria. *Annu. Rev. Microbiol.* **1997**, *51* (1), 527–564.
- (39) Yayarath, B.; AlonzoFreitag, F. N. E. F.; Freitag, N. E. Identification of a peptide-pheromone that enhances *Listeria monocytogenes* escape from host cell vacuoles. *PLoS Pathog.* **2015**, *11* (3), No. e1004707.
- (40) Eckert, R.; Qi, F.; Yarbrough, D. K.; He, J.; Anderson, M. H.; Shi, W. Adding selectivity to antimicrobial peptides: rational design of a multidomain peptide against *Pseudomonas* spp. *Antimicrob. Agents Chemother.* **2006**, *50* (4), 1480–1488.
- (41) Yang, S. T.; Shin, S. Y.; Hahm, K. S.; Kim, J. I. Design of perfectly symmetric Trp-rich peptides with potent and broad-spectrum antimicrobial activities. *Int. J. Antimicrob. Agents* **2006**, *27* (4), 325–330.
- (42) Wang, Y.; Cui, P.; Zhang, Y.; Yang, Q.; Zhang, S. Augmentation of the antibacterial activities of Pt5-derived antimicrobial peptides (AMPs) by amino acid substitutions: Design of novel AMPs against MDR bacteria. *Fish Shellfish Immunol.* **2018**, *77*, 100–111.
- (43) Wang, C.; Shen, M.; Gohain, N.; Tolbert, W. D.; Chen, F.; Zhang, N.; Yang, K.; Wang, A.; Su, Y.; Cheng, T.; Zhao, J.; Pazgier, M.; Wang, J. Design of a potent antibiotic peptide based on the active region of human defensin 5. *J. Med. Chem.* **2015**, *58* (7), 3083–3093.
- (44) Jia, X.; Ahmad, I.; Yang, R.; Wang, C. Versatile graphene-based photothermal nanocomposites for effectively capturing and killing bacteria, and for destroying bacterial biofilms. *J. Mater. Chem. B* **2017**, *5* (13), 2459–2467.
- (45) Tang, H.; Liu, Y.; Li, B.; Shang, B.; Yang, J.; Zhang, C.; Yang, L.; Chen, K.; Wang, W.; Liu, J. Water-soluble PANI:PSS designed for spontaneous non-disruptive membrane penetration and direct intracellular photothermal damage on bacteria. *Bioact. Mater.* **2021**, *6* (12), 4758–4771.
- (46) Zhu, X.; Dong, N.; Wang, Z.; Ma, Z.; Zhang, L.; Ma, Q.; Shan, A. Design of imperfectly amphipathic  $\alpha$ -helical antimicrobial peptides with enhanced cell selectivity. *Acta Biomater.* **2014**, *10* (1), 244–257.
- (47) Chou, S.; Shao, C.; Wang, J.; Shan, A.; Xu, L.; Dong, N.; Li, Z. Short, multiple-stranded  $\beta$ -hairpin peptides have antimicrobial potency with high selectivity and salt resistance. *Acta Biomater.* **2016**, *30*, 78–93.
- (48) Shan, J.; Li, X.; Yang, K.; Xiu, W.; Wen, Q.; Zhang, Y.; Yuwen, L.; Weng, L.; Teng, Z.; Wang, L. Efficient bacteria killing by  $\text{Cu}_2\text{WS}_4$  nanocrystals with enzyme-like properties and bacteria-binding ability. *ACS Nano* **2019**, *13*, 13797–13808.
- (49) Liu, Y.; Nie, N.; Tang, H.; Zhang, C.; Chen, K.; Wang, W.; Liu, J. Effective antibacterial activity of degradable copper-doped phosphate-based glass nanozymes. *ACS Appl. Mater. Interfaces* **2021**, *13* (10), 11631–11645.
- (50) Jiang, Z.; Vasil, A. I.; Gera, L.; Vasil, M. L.; Hodges, R. S. Rational design of  $\alpha$ -helical antimicrobial peptides to target Gram-negative pathogens, *Acinetobacter baumannii* and *Pseudomonas aeruginosa*: utilization of charge, 'specificity determinants,' total hydrophobicity, hydrophobe type and location as design parameters to improve the therapeutic ratio. *Chem. Biol. Drug Des.* **2011**, *77* (4), 225–240.
- (51) Chen, Y.; Guarnieri, M. T.; Vasil, A. I.; Vasil, M. L.; Mant, C. T.; Hodges, R. S. Role of Peptide Hydrophobicity in the Mechanism of Action of  $\alpha$ -Helical Antimicrobial Peptides. *Antimicrob. Agents Chemother.* **2007**, *51* (4), 1398–1406.
- (52) Zasloff, M. Magainins, a class of antimicrobial peptides from *Xenopus* skin: isolation, characterization of two active forms, and partial cDNA sequence of a precursor. *Proc. Natl. Acad. Sci. U.S.A.* **1987**, *84*, 5449–5453.
- (53) Javia, A.; Amrutiya, J.; Lalani, R.; Patel, V.; Bhatt, P.; Misra, A. Antimicrobial peptide delivery: an emerging therapeutic for the treatment of burn and wounds. *Ther. Delivery* **2018**, *9* (5), 375–386.
- (54) Annunziato, G.; Costantino, G. Antimicrobial peptides (AMPs): a patent review (2015–2020). *Expert Opin. Ther. Pat.* **2020**, *30*, 931–947.
- (55) Yeaman, M. R.; Yount, N. Y. Mechanisms of antimicrobial peptide action and resistance. *Pharmacol. Rev.* **2003**, *55* (1), 27–55.
- (56) Epanand, R. M.; Walker, C.; Epanand, R. F.; Magarvey, N. A. Molecular mechanisms of membrane targeting antibiotics. *Biochim. Biophys. Acta* **2016**, *1858* (5), 980–987.
- (57) Peschel, A.; Sahl, H.-G. The co-evolution of host cationic antimicrobial peptides and microbial resistance. *Nat. Rev. Microbiol.* **2006**, *4* (7), 529–536.